



TECHNOLOGICAL EDUCATIONAL
INSTITUTE OF CRETE

SCHOOL OF APPLIED SCIENCES



DEPARTMENT OF ENVIRONMENTAL AND NATURAL
RESOURCES ENGINEERING

Master of Science Course

“Geoenvironmental Resources & Risks”

THESIS

Application of Natural Time Analysis of Seismicity in
areas where Thermal Anomalies were observed by
Robust Satellite Techniques

Student

Alexandros Eleftheriou

Supervisors

Prof. Filippos Vallianatos

Prof. Valerio Tramutoli

Dr. Teodosio Lacava

Dr. Mariano Lisi

Dr. George Drakatos

Chania - Potenza 2016



UNESCO Chair
SOLID EARTH PHYSICS and GEOHAZARDS RISK REDUCTION
Technological Educational Institute of Crete, Greece
Head of the Chair, Dr. Filippos Vallianatos
Professor of Geophysics & Seismology
3 Romanou Str., Chania, GR 73100, Crete, Greece.
email : fvallian@chania.teicrete.gr

In collaboration with:



Dedicated to my Family and Friends

Αφιερωμένο στην Οικογένεια και τους φίλους μου

«Εκ των διαφερόντων καλλίστην αρμονίαν»

Ηράκλειτος

ACKNOWLEDGEMENTS

At this point, I would like to give my deepest gratitude to all the people that directly or indirectly helped me to fulfill this thesis. This study was made during my Erasmus Placement in Potenza, Italy, working with the scientific groups from the Institute of Methodologies for Environmental Monitoring (IMAA) and University of Basilicata (LADSAT Laboratory team). I'm glad to have this opportunity to express my sincere thanks for and appreciation of all the assistance that I have received. I would like to give my sincere thanks to Dr. Vincenzo Lapenna and Dr. Teodosio Lacava who accepted my application for my Erasmus placement. My deepest gratitude to my supervisors/professors Valerio Tramutoli and Filippos Vallianatos as well as Dr. Mariano Lisi and Dr. Teodosio Lacava that first of all offered me all I needed to have a great stay in Potenza and for their advice and corrections that helped me fulfill this study.

My thanks also goes to the LADSAT team, Carolina Filizzola, Rossana Paciello and Nicola Genzano for their guidance and support. Furthermore, I would like to express my sincere thanks to Sofia Peleli, Christina Kominou, Lorena Di Bello, Francesco Melfi, Gemma Cossidente, Serena Danese and Morgana Bruno for their support and for being there and share this experience with me.

I also wish to thank Antonia Reinhard for being there and that her guidance and support helped me overcome difficulties, for the influence and motivation she gave in my life.

Finally, and most important, I would like to express my deepest gratitude to my parents for all their support over the years and for being there whatever I needed. For trusting me and for loving me no matter what.

I am glad that I met and have spent time with all these people. Thank you everyone.

Contents

ACKNOWLEDGEMENTS	5
INTRODUCTION	7
Chapter 1	9
Natural time analysis and Robust Satellite Techniques	9
1.1 Natural time analysis	9
1.2 Robust Satellite Techniques (RST)	14
1.3 State of the art: Applications of NTA and RST to seismic hazard assessment ..	17
Chapter 2	27
RST and NTA implementation for long-term seismicity analysis of Greece.....	27
2.1 Long term RST analysis of TIR observations over Greece (RST).....	27
2.1.1 Correlation analysis with seismic events with $M > 4$	34
2.1.2 Correlation analysis by using a barycentral approach	35
2.1.3 Analysis of results.....	38
2.2 Long-term NTA analysis of seismic data over Greece (NTA)	46
2.2.1 Correlation analysis with strong seismic events.....	46
2.2.2 Analysis of results.....	48
Chapter 3	50
Multi-parametric analysis	50
3.1 Joint correlation analysis with seismic events ($M \geq 4$)	50
3.1.1 Analysis of results.....	51
Conclusions.....	57
References.....	59
Annex – Natural time analysis for strong Earthquake events.....	66

INTRODUCTION

Earthquakes are among the most dangerous and disastrous natural hazards. Yet, they poses a complex system at the basis of their occurrence, which makes them hard to forecast. A number of methodologies have been proposed and applied by scientists around the globe in different geotectonic systems in order to achieve a short-term seismic hazard assessment, but up to now, no single measurable parameter and/or no observational methodology has been able to provide useful information to make some kind of possible Earthquake prediction. Due to the complexity of the preparation phase of seismic events, the need for a multi-parametric observation arises.

Moving towards to such observations to improve short-term Earthquake forecast might be possible. Yet, is worth mentioning the importance of selecting suitable parameters and appropriate methods for data analysis in order to achieve such a prediction. A very preliminary step in this direction is the identification of those parameters (geodynamic, chemical, physical, etc.) whose space-time dynamics and/or anomalous variability can be, to some extent, associated with the process of preparation for major Earthquakes.

In addition, by combining and bringing together the scientific community and knowledge from interdisciplinary fields (i.e., atmospheric sciences, geophysics, seismology, electromagnetism researchers etc.) could benefit this kind of multi-parametric observations, give a better understanding on the complexity of the system and provide an integrated seismic hazard assessment.

The present study will deal just with two parameters, the thermal infrared signal and the seismicity, that will be analyzed by Robust Satellite Techniques and Natural Time Analysis respectively. Robust Satellite Techniques (RST) has been used as a suitable tool for study the anomalous fluctuation of Earth's emitted thermal infrared radiation (TIR) in seismically active areas and Natural Time Analysis (NTA) has been applied in time series of Earthquakes in order to provide information on when the system enters in a critical stage, prior to the occurrence of strong seismic events.

The thesis is organized in three chapters.

The first chapter will provide a brief introduction on the two methodologies (NTA and RST) as well as on the state of the art of their applications. Then, the implementation of both on long-term seismicity over Greece and the results will be discussed. Firstly,

an overview of the results of RST applied over Greece on a previous study and then the results of a new proposed approach. Secondly, the application of NTA on strong seismic events will be shown. In the last chapter the results of the multi-parametric approach will be analyzed and discussed in detail.

Chapter 1

Natural time analysis and Robust Satellite Techniques

Time is a crucial parameter for the preparation phase of an Earthquake. By better knowing, understanding it and taking into account other parameters, it will be possible to get a step closer to the big challenge, a short-term Earthquake prediction. In this chapter, after a brief introduction of Seismic Electric Signals and the concept of Natural Time Analysis (NTA), the Robust Satellite techniques (RST) methodology will be briefly explained as well as the state of the art of the two methodologies.

1.1 Natural time analysis

The VAN method was introduced and named after the two papers published by P. Varotsos, K. Alexopoulos and K. Nomicos in 1981 (Varotsos et al., 1981a, 1981b) where they described it. They showed that, when the pressure on an ionic solid¹ attains a critical state, a cooperative orientation of the electric dipoles may occur, which can result in the emission of a short-lived electric signal. Seismic Electric Signals (SES) are low frequency (≤ 1 Hz) changes of the electric field of the Earth and can be used as a precursor prior to Earthquakes, that can be observed within a time window from some hours to a few months before the seismic event (Varotsos et al., 1986, 2001) (Figure 1.1).

The experimental methodology for measuring the SES is explained below. Two electrodes are inserted into the ground, in a depth of about a meter. Each electrode is connected to one end of an insulated cable and then the potential difference is measured between the two free ends of the wires with a voltmeter. The potential difference between two points A and B on the Earth's surface is measured. This measured system is called electric dipole. When the SES is detected, the potential difference between the two points, changes by ΔV , the ratio $\Delta V/L$, obtained dividing this value by the distance L between the two electrodes gives the change of the electric field of the Earth in the direction AB. In order to search the reliability of the Earth's electric field change, at least a further measurement has to be taken simultaneously in a second direction, for example the one that is perpendicular to AB. From a practical point of view, several dipoles are necessary to be able to distinguish signals coming from natural sources (and

¹ Ionic Solids are solids composed of oppositely charged ions. They consist of positively charged cations and negatively charged anions.

in particular the SES emitted from natural sources, such as, the focal areas of future Earthquakes) and the signals coming from “artificial” sources, i.e. electrical installations from nearby industrial areas or the electrochemical changes of the electrodes due to rain. To achieve this distinction, therefore, for each direction many measuring dipoles of different lengths are used, for example 200 meters, 1 km, and 10 km. When the signal is recorded, each direction is checked, looking in particular if the ΔV values measured are proportional to the corresponding lengths. When the ratio $\Delta V/L$ is constant for all dipoles (short and long) of each direction, the signal cannot be attributed to an “artificial” source at a distance of up to several kilometers (Lazaridou – Varotsos, 2013).

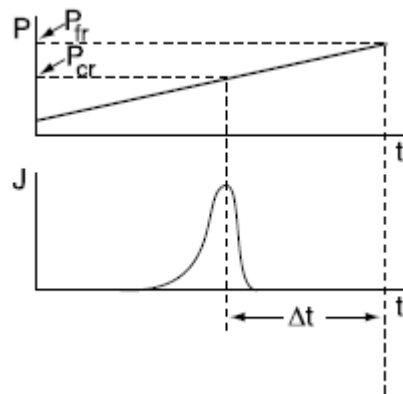


Figure 1.1 Schematic diagram of Varotsos and Alexopoulos' theory, which shows that before the fracture an electrical signal is emitted. The upper figure shows that the pressure (stress) (P) exerted on a solid gradually increases versus time (t) and when it reaches a critical value (P_{cr}) then a transient electrical signal of intensity J is emitted, shown in the figure below. The figure also shows that the fracture (fr) of the material occurs after some time Δt , i.e., when the pressure (stress) reaches a value P_{fr} that is greater than the critical pressure P_{cr} . At low pressure, the electric dipoles have random orientations, and just when all dipoles acquire the same orientation, the solid emits a warning signal, which constitutes the SES (Varotsos et al., 2001).

A number of measurements of the electric field of the Earth have been performed in Greece since the 80's to assess the validity of the methodology. Today, several SES stations are operating in Greece providing real-time measurements, giving information on the transient electric signals (Figure 1.2).

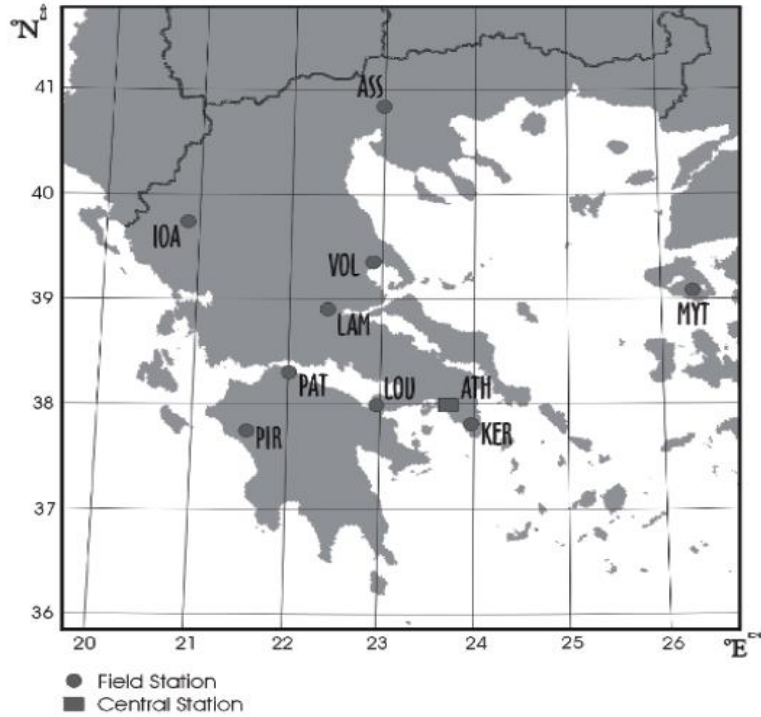


Figure 1. 2 Map showing the sites of the stations of the real-time telemetric network currently operating in Greece (Mary S. Lazaridou – Varotsos, 2013).

On the basis of SES activity, Varotsos et al., (2001) introduced a new time domain, different from the conventional time t , termed natural time χ , in order to show that the interrelation which exists between the time evolution of the seismic activity (starting measuring it from the first SES recording) and the spectrum characteristics of the SES can be achieved when looking at both of them in this new time domain.

Natural time, in a time series of N events, can serve as an index for the occurrence of an event (divided by the total number of events, therefore being less than, or equal to 1).

$$\chi_k = \frac{k}{N} \quad (1.1)$$

where k represents each time of the occurrence of the new event and N the total number of events.

There are other quantities contemplated in natural time, such as Q_k , which is a quantity corresponding to the energy of the specific event. Starting from Q_k the quantity p_k can be considered as (Varotsos et al., 2011):

$$p_k = \frac{Q_k}{\sum_{n=1}^N Q_n} \quad (1.2)$$

$$\sum_{k=1}^N p_k = 1 \quad (1.3)$$

where p_k is the normalized energy that is emitted in the time of the individual (k -th) event. Thus, in natural time the evolution of the pair either (χ_k, Q_k) or (χ_k, p_k) is considered.

In the case of seismicity, the evolution of the pair (χ_k, M_k) is considered, where M_k is the seismic moment (which is proportional to the energy emitted in the specific Earthquake, $M_k \propto 10^{cM}$ where $c \approx 1.5$) released during the k -th event (Figure 1.3).

In the following, the order parameter, proposed for seismicity is introduced starting with the assumption that a mainshock can be considered as the new phase.

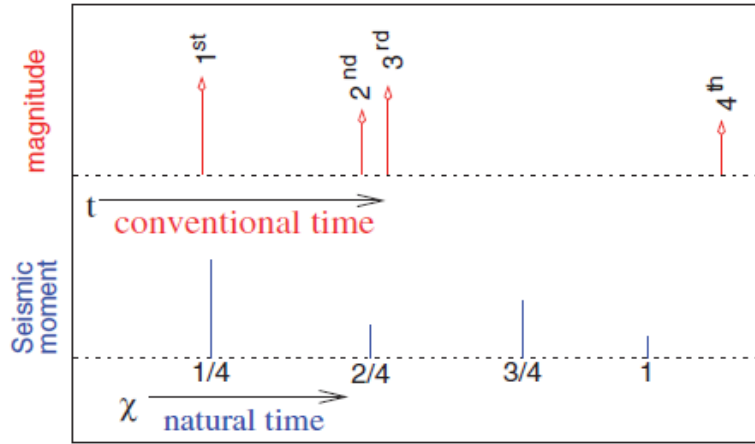


Figure 1. 3 How a series of seismic events in conventional time t (upper panel, red) can be read in natural time χ (lower panel, blue) (Varotsos et al., 2011).

Regarding the evolution of (χ_k, M_k) , the continuous function $F(\omega)$ is defined as:

$$F(\omega) = \sum_{k=1}^N M_k \exp(i\omega \frac{k}{N}) \quad (1.4)$$

where $\omega=2\pi\varphi$ and φ stands for the natural frequency². Then, in order to normalize $F(\omega)$ it has to be divided by $F(0)$. Thus:

$$\Phi(\omega) = \frac{\sum_{k=1}^N M_k \exp(i\omega \frac{k}{n})}{\sum_{n=1}^N M_n} = \sum_{k=1}^N p_k \exp(i\omega \frac{k}{N}) \quad (1.5)$$

where $p_k = \frac{M_k}{\sum_{k=1}^N M_n}$. The quantities p_k describe the probability to observe an

Earthquake event at natural time χ_k . From equation (1.5) the normalized power spectrum can be obtained: $\Pi(\omega) = |\Phi(\omega)|^2$. (Varotsos et al., 2011) proved that for natural frequencies $\varphi < 0.5$, $\Pi(\omega)$ or $\Phi(\omega)$ reduces to a characteristic function for the probability distribution p_k in the context of probability theory and so the following relation derives:

$$\Pi(\omega) = \frac{18}{5\omega^2} - \frac{6\cos\omega}{5\omega^2} - \frac{12\sin\omega}{5\omega^3} \quad (1.6)$$

In consonance with probability theory, the moments of a distribution and hence the distribution itself can be approximately determined once the behavior of the characteristic function of the distribution is known around zero. Thus, for $\omega \rightarrow 0$, the equation (1.6) leads to:

$$\Pi(\omega) \approx 1 - \kappa_1 \omega^2 \quad (1.7)$$

where κ_1 is the variance in natural time, given as

$$\kappa_1 = \langle x^2 \rangle - \langle x \rangle^2 = 0.070 \quad (1.8)$$

Thus, analyzing the seismicity by computing the normalized power spectrum $\Pi(\varphi)$ on the basis of natural time and the variance κ_1 we can see, if and when the system enters in a critical point. In general, before a mainshock, a sequence of Earthquakes occurs, that obeys the equation (1.6). When the mainshock occurs, $\Pi(\varphi)$ abruptly increases to approximately unity and κ_1 becomes almost zero. The coincidence that the normalized power spectrum $\Pi(\varphi)$ and the variance κ_1 reaches the aforementioned values occurs usually some days to around a week before the main event (Varotsos et al., 2011).

² The frequency at which a system oscillates when not subject to a continuous or repeated external force.

1.2 Robust Satellite Techniques (RST)

The RAT (Robust AVHRR Technique) approach (Tramutoli, 1998) is a multi-temporal scheme of satellite data analysis proposed to study different natural/environmental hazards (e.g. Earthquake, floods, forest fires, oil spill, volcano, etc.).

This approach considers every anomaly in the space-time domain as a deviation from a “normal” state, which may be determined processing cloud-free satellite records, selected on the basis of specific homogeneity criteria (i.e. same sensor, same geographic area, same spectral channel/s, same recording period, e.g. month and acquisition time). Signal measured by satellite depends indeed on several factors, such as the physical properties of the target and the environmental/observational conditions (e.g. land cover, atmospheric conditions, hour of the day, geometry of observation, illumination). Therefore, if the signal variability in space and time domains is not taken into account, actual anomalous events should be more effectively identified. An index named ALICE (Absolutely Local³ Index of Change of the Environment) is then computed by RAT to this aim, and defined in its general mathematical formulation as:

$$\otimes_v(x, y, t) = \frac{[V(x, y, t) - V_{REF}(x, y)]}{\sigma_v(x, y)} \quad (1.9)$$

In this equation $V(x, y, t)$ is the signal measured at time t for each pixel (x, y) of the satellite image to process, $V_{REF}(x, y)$ is the expected value (generally expressed as the temporal mean), and $\sigma(x, y)$ is the natural variability of the signal (i.e. the temporal standard deviation). Thus, higher the ALICE index values, stronger the anomaly intensities. The robustness of such an approach is intrinsic, because a signal will be identified as “anomalous” only if it is higher than its expected value, for a specific condition of observation, and only if this deviation (i.e. the numerator in equation 1.9) is significantly higher than the natural signal variability (i.e. the signal fluctuations observed, in the time series, in absence of any perturbing effect).

³ The double l was introduced in (Tramutoli, 1998), to highlight a reference not only to a specific place r but also to a specific time t' .

The RAT approach was renamed RST (Robust Satellite Techniques) by Tramutoli (2005) to better emphasize its applicability to whatever satellite sensor data used. Among its different applications, RST was applied to seismic hazard analysis and in particular, to isolate possible pre-seismic TIR anomalies from signal variations (Table 1.1) due to natural and/or observational factors (natural/observational noise).

Table 1. 1 Main natural and observational factors affecting TIR signal (adapted from Tramutoli et al., 2005)

Main factors contributing to TIR signal variability	Description
a) Surface spectral emissivity	Quite constant (~0.98) on oceans. Over land it is highly variable taking values within 0.90 and 0.98 mainly depending on soil vegetation
b) Atmospheric spectral transmittance	Depends mainly on atmospheric temperature and humidity vertical profiles
c) Surface temperature (temporal variations)	Related to the regular daily and yearly solar cycles but sensitive also to meteorological (and climatological) factors
d) Surface temperature (spatial variations)	Depend on local geographical (altitude above sea level, solar exposition, geographic latitude) factors
e) Observational conditions (spatial variations)	Variations across the same scene of satellite zenithal angles introduce spatial variations of the registered signal not related to real near-surface thermal fluctuations
f) Observational conditions (temporal variations of satellite view angle) ^a	The same location is observed, at each revisiting time, at a different satellite zenithal angle: this introduces a spurious temporal variation of the measured signal due simply to the change in observational conditions (e.g. air mass)
g) Observational conditions (temporal variations of ground resolution cells) ^a	The change of satellite view angle also determines a sensible change in the size of the ground resolution cell. Spurious temporal variations of the measured signal have to be expected then because of the change in size of the ground resolution cell
h) Observational conditions (variations of the time of the satellite pass) ^a	Satellite pass occurs each day at different times falling in a time-slot up to 3 hours around the nominal time of pass. Spurious variations of the measured signal have to be then

expected as a consequence of such (time) variability of observation condition

^a Only for instrumental packages onboard of polar satellite (not applicable to geostationary platforms)

In the case of TIR anomalies possibly associated to seismic events, the Robust Estimator of TIR Anomalies (RETIRA) (Filizzola et al., 2004; Tramutoli et al., 2005) index was introduced:

$$\otimes(\mathbf{r}, t') = \frac{[\Delta T(\mathbf{r}, t') - \mu_{\Delta T}(\mathbf{r})]}{\sigma_{\Delta T}(\mathbf{r})} \quad (1.10)$$

Where:

- $\mathbf{r}=(x, y)$ represents pixel coordinates on satellite image;
 - t' is the time of acquisition of the satellite image at hand, with ($t' \in \tau$) where τ defines the homogeneous domain of satellite imagery collected in the same time (hour) of the day and period (month) of the year;
- $\Delta T(\mathbf{r}, t')=T(\mathbf{r}, t')-\langle T(t') \rangle$ is the difference between the current ($t=t'$) TIR signal $T(\mathbf{r}, t')$ measured at location \mathbf{r} , and its spatial average $\langle T(t') \rangle$, computed in place on the image at hand, discarding cloudy pixels and considering only sea pixels, if \mathbf{r} is located on the sea, only land pixels, if \mathbf{r} is located over the land⁴.
- $\mu_{\Delta T}(\mathbf{r})$ and $\sigma_{\Delta T}(\mathbf{r})$ are the time average and standard deviation values of $\Delta T(\mathbf{r}, t)$, at location \mathbf{r} , computed on cloud-free satellite records belonging to selected homogeneous data-set ($t' \in \tau$).

The $\otimes(\mathbf{r}, t')$ index gives the spatial-temporal local (*llocal*) excess of the current $\Delta T(\mathbf{r}, t')$ signal compared with its historical mean value and weighted by its historical variability at the considered location. Both $\mu_{\Delta T}(\mathbf{r})$ and $\sigma_{\Delta T}(\mathbf{r})$ are computed for each location \mathbf{r} , by processing several years of historical satellite records acquired under similar observational conditions. The excess $\Delta T(\mathbf{r}, t') - \mu_{\Delta T}(\mathbf{r})$ then represents the

⁴ The choice of such a differential variable $\Delta T(\mathbf{r}, t')$ instead of $T(\mathbf{r}, t')$ is expected to reduce possible contributions (e.g. occasional warming) due to day-to-day and/or year-to-year climatological changes and/or season time-drifts.

signal (S) which is to be investigated for its possible relation with Earthquake space-time occurrence. It is always evaluated by comparison with the corresponding natural/observational noise (N), represented by standard deviation, $\sigma_{\Delta T}(\mathbf{r})$. In this way, the intensity of anomalous TIR transients can be evaluated in terms of S/N ratio by the $\otimes(r, t')$ index. Tramutoli et al., (2001) reported that, the use of RETIRA index should highlight the presence of thermal anomalies effectively independent from the known sources of natural/observational noise, also in very low intensity.

1.3 State of the art: Applications of NTA and RST to seismic hazard assessment

Both NTA and RST approaches have been used to improve short-term Earthquake forecast. They have already been applied in different areas around the Earth on different seismic environments (namely, Italy, Japan, Greece, Turkey, etc.). Considering the purpose of this study, in the following only the applications of the two methodologies over Greece will be mostly mentioned.

The work that was discussed in Varotsos et al. (2011), was one of the first studies where the concept of Natural time analysis was applied to investigate the evolution of seismicity before the strong Earthquake occurred on May 13, 1995 with magnitude $M_w=6.6$ at Grevena-Kozani, Greece. As mentioned before, a crucial point for this approach is to establish the time when starting to analyze the seismicity. In the work, the authors decided to start the analysis immediately after the SES activity on April 18, 1995. Therefore, firstly, they converted the magnitudes of each event into the corresponding seismic moments and then plotted the results in the natural time domain (Figure 1.4). The total number of Earthquakes occurred in the defined area were 18, including the mainshock.

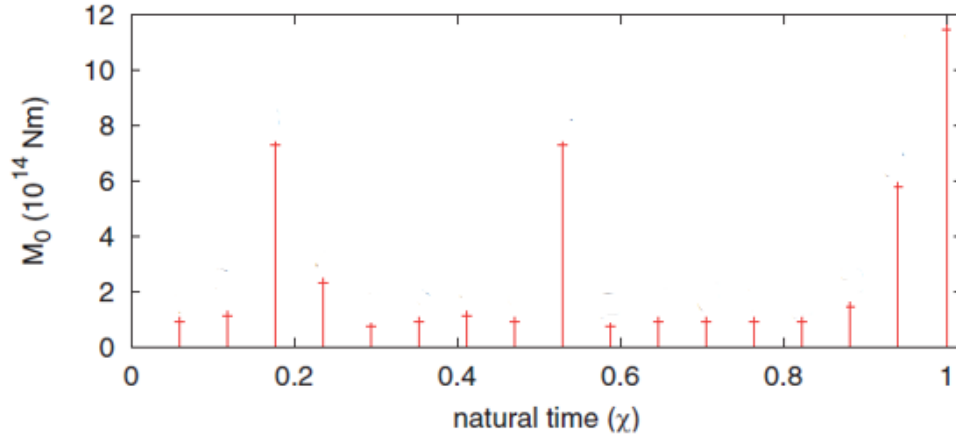
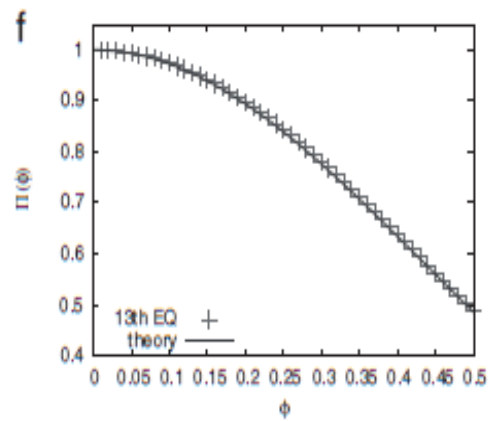
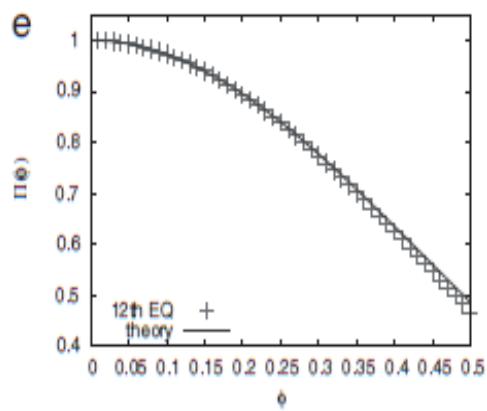
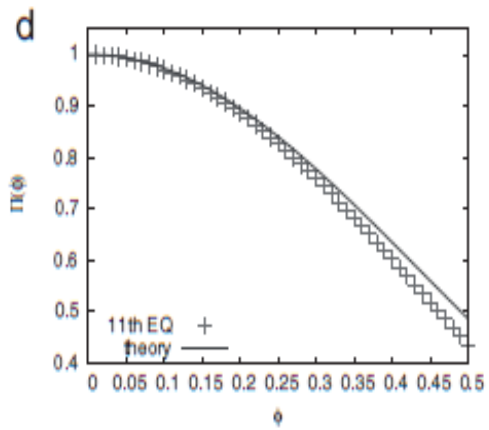
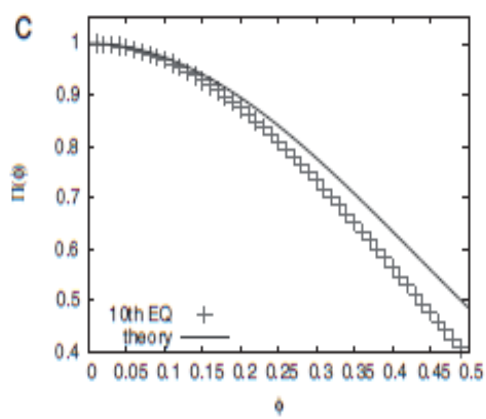
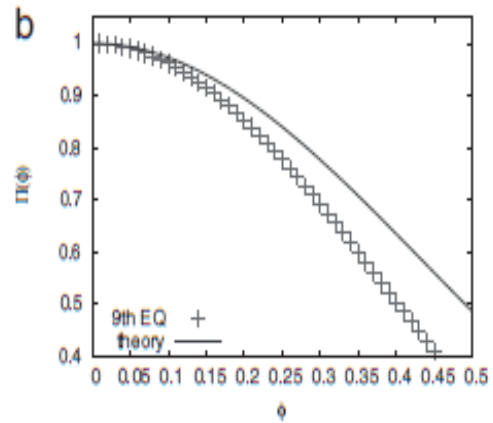
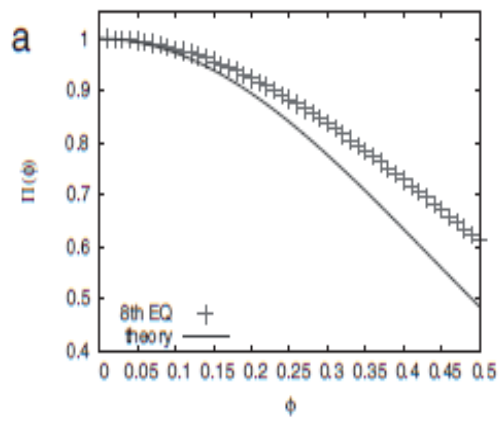


Figure 1. 4 Plot in natural time of the events that occurred after the initiation of the SES activity on April 18, 1995, until the mainshock on May 13, 1995 (Varotsos et al., 2011).

Then, the values of the normalized power spectrum $\Pi(\varphi)$ were calculated for natural frequencies $\varphi \in [0,0.5]$ as they progress upon the occurrence of each new event (following the methodology and equations explained before). In Figure 1.5 are plotted the results of the analysis. It can be seen that upon the occurrence of the 9-th event, the crosses (results from the normalized power spectrum) start to approach the solid line which represents equation 1.6 (Figure 1.5c). The cross line almost coincide when the 12-th event occurs, on May 10 (Figure 1.5e), where the value of k_1 is close to 0.070 and is 3 days before the mainshock. Upon the mainshock the value of k_1 abruptly changes, turning to a straight line almost parallel to the horizontal axis. This change motivated the authors to consider k_1 as an order parameter for seismicity and hence showing when the system enters in a critical point.



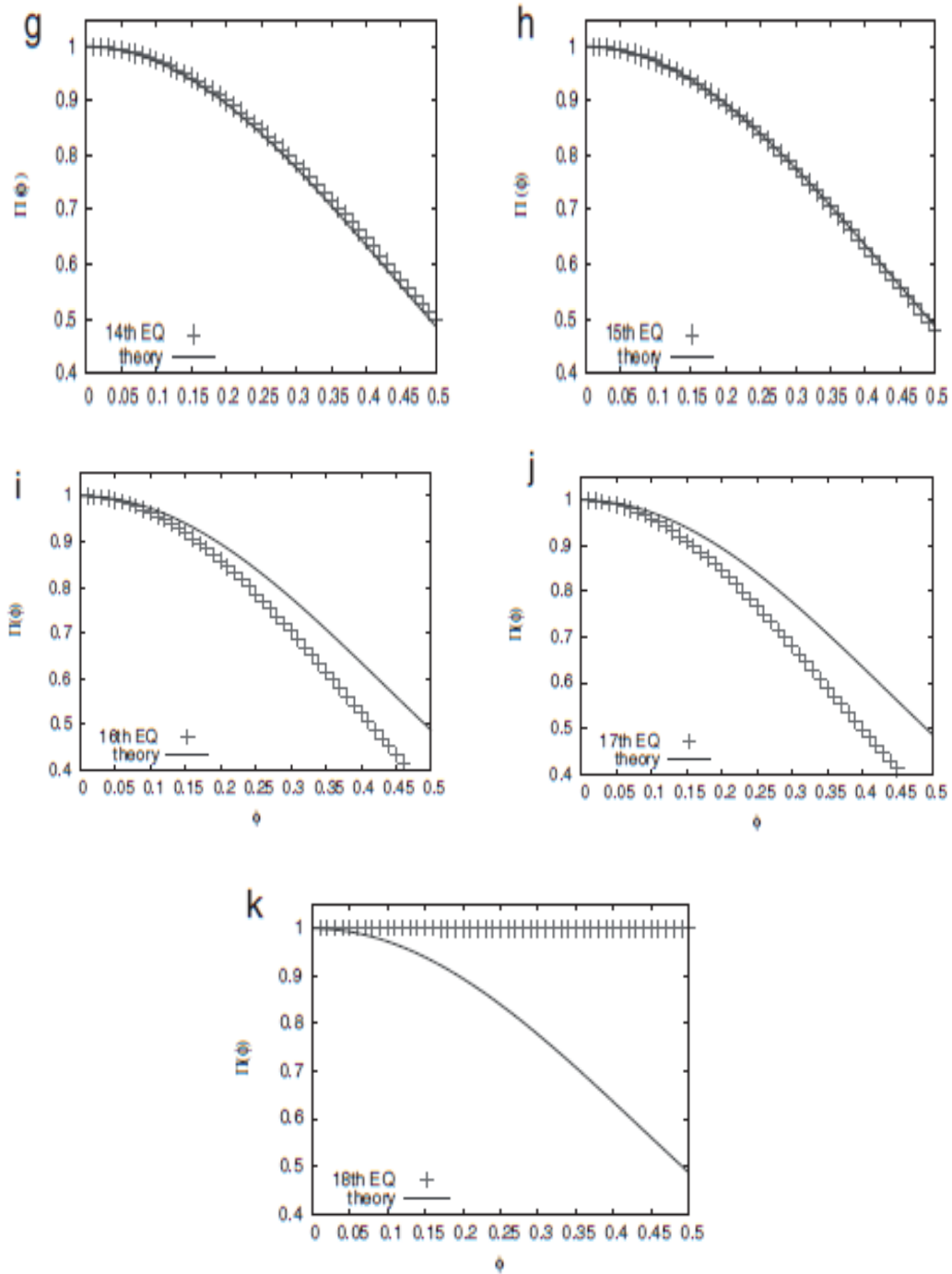


Figure 1. 5 Excerpts of the evolution of $\Pi(\phi)$ (crosses) of the seismicity that occurred after the initiation of the SES activity on April 18, 1995, until the mainshock of May 13, 1995. Figures (a) to (k) correspond to the $\Pi(\phi)$ versus ϕ results (crosses) upon the occurrence of each of the EQs from the 8-th to 18-th. (Adapted from Varotsos et al., 2011).

In another study, regarding Natural time analysis, (Sarlis et al., 2008), investigated the behavior of seismicity in the area candidate to suffer a main shock after the observation of the Seismic Electric Signal activity until the impending mainshock. They mentioned, that, both SES emission and Earthquake occurrence are critical phenomenon and that the approach to “electrical” critical point shortly precedes the approach to “mechanical” critical point is a fundamental premise for short-term Earthquake prediction. In this study they presented a new method using natural time for shortening the time-window of short-term Earthquake prediction. Furthermore, a new approach regarding the selection of the area candidate for the impending mainshock was also introduced. In particular, after selecting the first candidate area around the SES station where the signal was observed and the order parameter reached criticality, they created additional subareas (with a rectangular geometry) to follow investigating the seismicity and construct the probability (k_1) versus k_1 graph to examine whether it maximizes at $k_1 \approx 0.07$. A subset is qualified as a proper subset only if it includes all Earthquakes that took place inside its corresponding rectangular subarea (Figure 1.6). They applied this approach in different case studies, where, there was SES activity in Greece. Results shown that following the subsequent seismicity, the probability density function of k_1 is obtained, which maximizes at $k_1 \approx 0.07$ usually around a few days before the occurrence of the main shock.

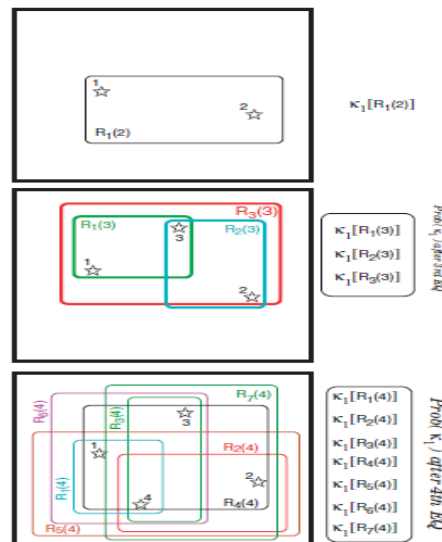


Figure 1. 6 The area A (in thick black rectangle) and its rectangular subareas $R_j(i)$, corresponding to the proper subsets immediately after the occurrence of the second Earthquake “2” (upper panel), the third Earthquake “3” (middle panel) and the fourth Earthquake “4” (bottom panel). The location of each event is shown by an

open star. Right column shows that k_1 values can be obtained for each subset (Sarlis et al., 2008).

In order to show that the methodology is also applicable in different parts of the Earth, Varotsos et al., (2010) applied the natural time analysis on Earthquake data in USA for which clear precursory electromagnetic variations were reported almost one month before the 18 October 1989 Loma Prieta (California) Earthquake ($M_s=7.1$). They analyzed in natural time all the events that occurred after 12 September 1989, which is the date of the initiation of the precursory magnetic-field change, for an area centered on the epicenter (the shaded area in Figure 1.7). Choosing as magnitude threshold $M_{\text{thres}}=2.6$ in order to have homogeneous and complete catalog and repeating the calculation for larger magnitude thresholds in order to exhibit spatial and magnitude threshold invariance. The results shown that the probability k_1 maximizes at $k_1=0.07$ almost five days before the mainshock.

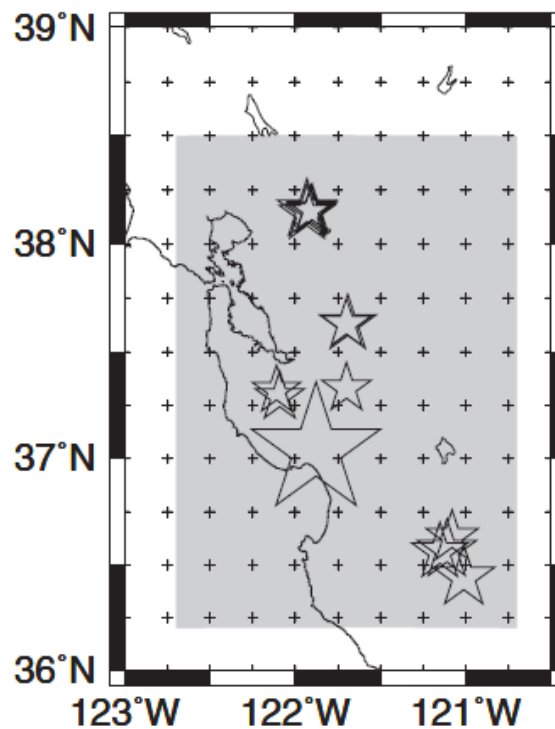


Figure 1. 7 A map of the area (shaded) surrounding the epicenter of the Loma Prieta Earthquake (large star) in which the seismicity after the initiation on 12 September 1989 of the precursory magnetic-field variations is analyzed in natural time (Varotsos et al., 2010).

Varotsos et al. (2015) using natural time analysis on the seismicity prior to an $M_w=5.4$ Earthquake that occurred in Greece on 17 November 2014 revealed that the system approached the critical point just a few days before the mainshock. In particular, the

initiation of natural time analysis of the seismicity was when a SES activity was recorded on 27 July 2014 at Keratea geoelectrical station. The candidate area can be seen in Figure 1.8 as well as the SES recordings. The seismicity was studied in that area, choosing events with a magnitude threshold $M_{\text{thres}}=2.8$. During that period, six smaller Earthquakes occurred and they observed that probability k_1 maximizes at $k_1=0.070$ upon the occurrence of the last Earthquake, with $M_L=2.8$ at 01:01 UT on 15 November 2014. The same study was performed with different magnitude thresholds and revealed a similar behavior of the probability k_1 , reaching criticality almost 3 days before the mainshock.

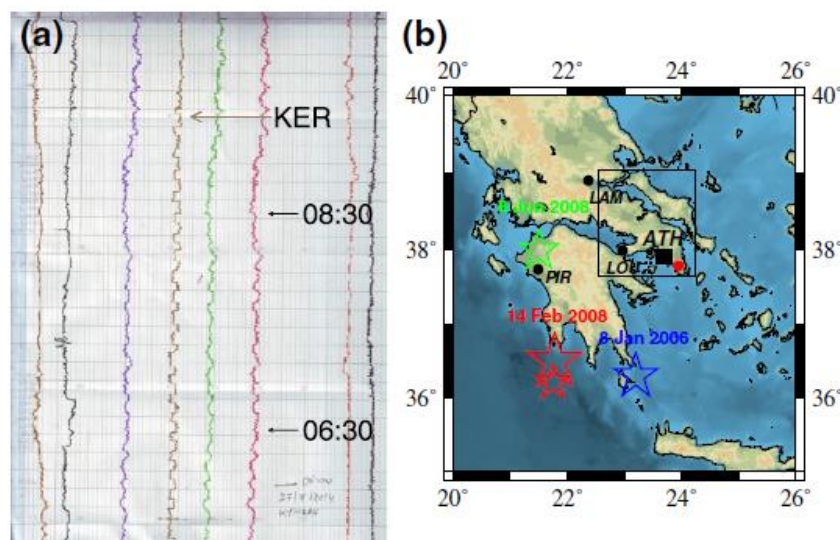


Figure 1. 8 a The SES activity of dichotomous nature recorded at the Keratea (KER) geoelectrical station of the SES telemetric network. b The predicted epicentral area designated by the rectangle on a map in which the location of the KER station (red bullet) is shown along with that of other geoelectrical stations Lamia (LAM), Loutraki (LOU) and Pirgos (PIR) (black bullets). The epicenters of the strongest Earthquakes in Greece ($M_W \geq 6.5$) during the last decade are also shown with stars. The central station of the SES telemetric network is located at Athens (ATH, black square) (Adapted from Varotsos et al., 2015).

In natural time analysis, it is very important to define the starting point for analyzing the seismicity around the area of the impending Earthquake. In a recent study Vallianatos et al., (2015) showed another approach to define such a starting point. Notably, they used a multi-resolution wavelet analysis (MRWA) on the inter-event times of the seismicity prior to the mainshock in order to examine the time variation of the standard deviation of wavelet coefficients. They showed that a decrease at lower

scales (usually appearing around 12 days prior to the main event) can be used as a time marker for the initiation of natural time analysis. Implementing this approach, they studied the seismicity prior to an Earthquake with $M_w=6.1$ on January 26, 2014, occurred in Cephalonia, Greece. Strong evidence of criticality in seismicity was observed within a few days before the main event. The probability k_1 of seismicity in natural time domain coincided with the theoretical curve of critical phenomena a few days before the $M_w=6.1$ event, for $M_{\text{thres}}=2.0$ magnitude threshold (Figure 1.9).

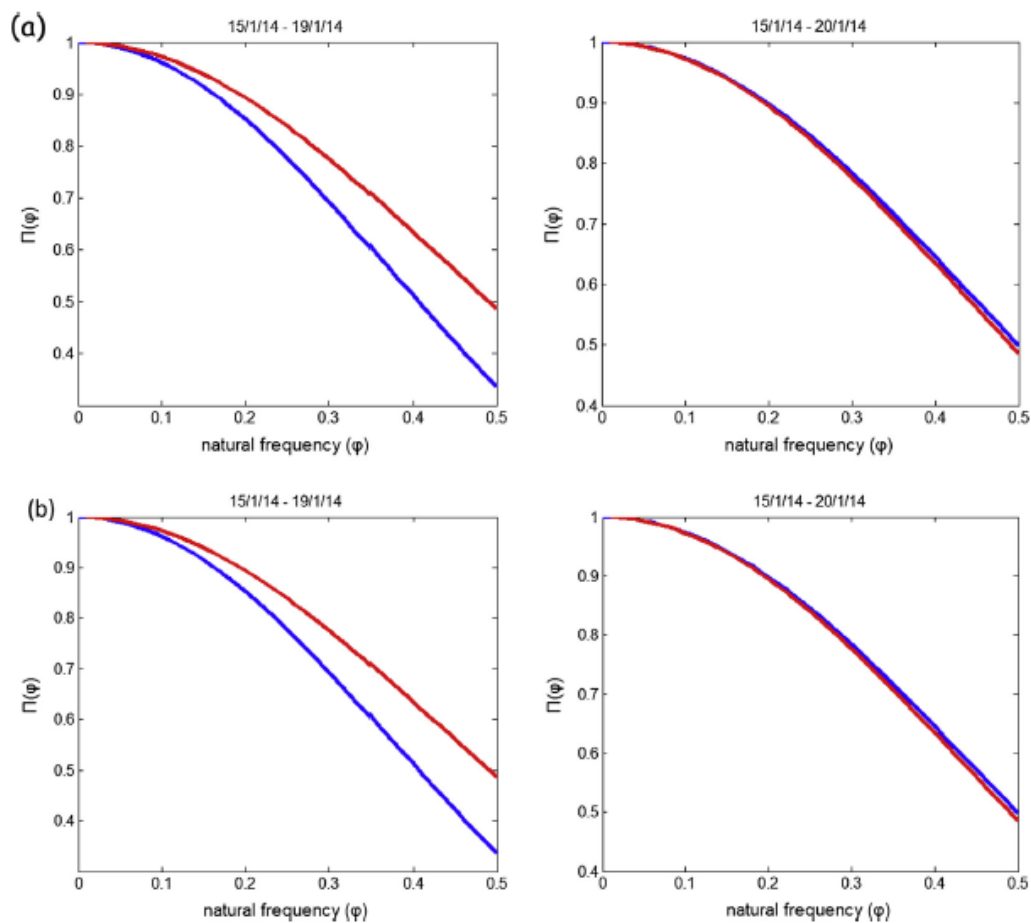


Figure 1. 9 Time evolution of $\Pi(\varphi)$ for $0 \leq \varphi \leq 0,5$ of the seismic activity for (a) $M_L \geq 2.0$ and $R = 30$ km, (b) $M_L \geq 2.0$ and $R = 50$ km, when the calculation was started on January 15, 2014. $\Pi(\varphi)$ curves (blue) fall on the theoretical $\Pi(\varphi)$ curve (red) as critical stage is approached (Vallianatos et al., 2015).

RST has been extensively used on investigating the potential of the thermal infrared (TIR) signals emitted from the Earth to provide Earthquake precursors. More than 10 years of applications of the general RST (Tramutoli 1998, 2005, 2007) methodology, have shown the ability of this approach to discriminate anomalous TIR signals possibly associated with seismic activity from normal fluctuations of Earth's thermal emission

related to other causes (e.g., meteorological) independent of the Earthquake occurrences. Being based on a statistical definition of TIR anomalies and on a suitable method for their identification even in very different local (e.g., related to atmosphere and/or surface) and observational (e.g., related to the time/season or satellite view angles) conditions, RST approach has been widely applied to tens of Earthquakes, covering a wide range of magnitudes (from 4.0 to 7.9) and very different geo-tectonic contexts (compressive, extensional, and transcurrent) in four different continents. RST intrinsic exportability permitted its implementation on TIR images acquired by sensors on board of different polar (see Filizzola et al., 2004; Lisi et al., 2010; Tramutoli et al., 2001) and geostationary satellites (see Corrado et al., 2005; Genzano et al., 2007, 2009a, b, 2010, 2015; Tramutoli et al., 2005).

The study of Filizzola et al. (2004) demonstrated, in the case of Athens's Earthquake (7 September 1999, $M_S=5.9$), the possibility to reach S/N ratios up to 1.5 by using daily RETIRA indexes $\otimes_{\Delta LST}(\mathbf{r}, t)$. In that case, the authors, using sequences of daily AVHRR images reported the appearance of (space-time) persistent TIR anomalies in the epicentral area some days before the seismic event.

Corrado et al., (2005) performed a sensitivity analysis on low magnitude Earthquakes in Greece and Turkey. In particular, 9 medium-low magnitude ($4 < M_b < 5.5$) Earthquakes which occurred in Greece and Turkey were analyzed in order to verify if TIR anomalies can be observed. By analyzing 8 years of satellite data (MSG, TIR observations) they concluded that TIR anomalies can be observed even in the presence of medium-low magnitude events. In Genzano, (2014), who applied for the first time a long period analysis over Italy, a few improvements to the standard approach were done. That study showed, the presence of 51 TIR sequences, of which 23 were in a space-time relations with Earthquakes (with $M \geq 4$) occurred in the same area and period and also the presence of 28 TIR sequences independent from the seismicity, but due to other phenomenon (known and unknown).

The papers just described are just a few of the studies which have been used for seismic hazard assessment on the basis of the two methodologies (NTA and RST) before introduced. Regarding NTA, the approach of the system in a critical stage can be seen usually from a week to a few days prior to the mainshock. Nevertheless, is worth mentioning the difficulty of selecting the starting point of the seismic data to be

analyzed and especially without knowing the epicenter of the impending mainshock. On the other hand, RST can detect thermal anomalies prior to strong Earthquakes up to one month before the occurrence of the event but with a main limitation when the scene is mostly cloudy. Hence, in order to have a better understanding on the preparatory phase of an impending strong Earthquake, this study is focused on the correlation of the two methodologies in an attempt to achieve a better short-term Earthquake forecast. In the following chapter, after a brief summary about the previous long term RST analysis of TIR observations over Greece, the new analysis regarding the barycenter of thermal anomalies will be discussed as well as the natural time analysis that was performed on the seismicity around the area of the observed thermal anomalies.

Chapter 2

RST and NTA implementation for long-term seismicity analysis of Greece

In this chapter, more details about the parameters and methods at the basis of the two methodologies used in this work (i.e., RST and NTA) will be provided as well as all the results achieved by implementing them on the night-time TIR images and the seismicity in the investigated area. Such a preliminary statistical analysis will provide evidences about any seismic precursors possible identifiable by RST and NTA.

2.1 Long term RST analysis of TIR observations over Greece (RST)

RST has been recently applied (Eleftheriou et al., 2015), on all (3151) TIR images acquired by MSG/SEVIRI satellite sensor in the IR10.8 channel (9.80–11.80 μm) in the first time slot of the day (00:00 \div 00:15 GMT; i.e., 02:00 \div 02:15 LT) since May 2004 up to December 2013. Night-time TIR images were preferred because less influenced by effects related to soil–air temperature differences (which are normally higher during other hours of the day) and less sensitive to local variations (due for instance to cloud cover or shadows) of solar illumination which could represent a further element of variability of TIR signal, independent from seismicity.

For each month a multi-annual homogeneous data set of TIR satellite images was built to compute 24 reference fields (one, $\mu_{\Delta T}$ plus $\sigma_{\Delta T}$, for each of the 12 calendar months) for a testing area (top-left 42.1°N—19.2°E; top-right 42.7°N—30.4°E; bottom-right 33.9°N—26.1°E; bottom-left 33.5°N—16.7°E) which includes the whole Greek peninsula. Following RST prescriptions, the computation of reference fields was made considering only the cloud-free pixels. In fact, thick meteorological clouds are not transparent to the passage of the Earth's emitted TIR radiation so that measured signal in those pixels refers to the cloud top temperature (usually very low) and not to the near surface conditions. Errors in the identification (and the consequent non-exclusion) of cloudy pixels, could heavily condition the quality of reference fields which, in general, will result biased toward lower values of averages $\mu_{\Delta T}(x,y)$ and higher values of

standard deviations $\sigma_{\Delta T(x,y)}$. Even if the latter effect - increasing the denominator of expression - could compensate the first one (increasing the numerator of the same expression) - avoiding, thanks to the robustness of RETIRA index, a proliferation of false positives, a significant reduction of the overall sensitivity can be however observed as a consequence of cloudy pixel identification errors.

In order to identify and discard from reference field computation cloudy affected pixels, the OCA (One-channel Cloudy-radiance-detection Approach; Pietrapertosa et al., 2001; Cuomo et al., 2004) method was used. Such a method, still RST based, and hence devoted to identify as cloudy those radiances which deviate significantly from the expected values for a specific place and time of observation, was preferred to traditional cloud detection methods (devoted to identify pixels containing clouds) which are much more exposed to commission (i.e., classifying pixels as cloudy independently if clouds affect or do not affect the measured radiance in the considered spectral band) and omission (mostly because of the use of a fixed threshold approach) errors (see for instance Pietrapertosa et al., 2001; Tramutoli et al., 2000). However, due to their importance, particular attention has been paid to cloudy pixel handling, introducing the following refinement of the standard RST pre-processing phases. In order to be sure that only cloud-free radiances contribute to the computation of reference fields, after cloudy pixels have been identified by OCA, not only those pixels but also the 24 ones in a 5×5 box around it (very often belonging to cloud edges) have been excluded by the following computations of reference fields (like in Eneva et al. 2008). As shown by Aliano et al., (2008a) and Genzano et al., (2009a), the spatial distribution of clouds over a thermally heterogeneous scene, can significantly change the value of the measured signal $\Delta T(x,y,t) = T(x,y,t) - T(t)$ in the remaining (cloud-free) pixels of the scene belonging to the same land/sea class. In fact, the same $T(x,y,t)$ value of measured TIR signal can be associated with an higher or lower $\Delta T(x,y,t)$ values depending on the spatial average $T(t)$ computed on the remaining cloud-free pixels (belonging to the same land/sea class of the pixel centered at the x, y coordinates). It has been shown - firstly by Aliano et al., (2008a) and then by Genzano et al., (2009a) who named it *cold spatial average effect* - that, if clouds mostly cover the warmer part of the land (or sea) portion of the scene, the spatial average $T(t)$ will result lower than expected in clear sky conditions. As a consequence anomalously higher values of the signal $\Delta T(x,y,t) = T(x,y,t) - T(t)$ can be measured over the remaining, cloud-free, land (or sea), portion of

the scene which are due only to such an anisotropic distribution of clouds along the North–South direction. If not properly taken into account, such a pure meteorological phenomenon not only could (occasionally) introduce false positives in the interpretation phases but will also strongly affect $\mu_{\Delta T}(x,y)$ and $\sigma_{\Delta T}(x,y)$ reference fields which will be both biased toward higher values with a strong reduction of the overall sensitivity of RETIRA index. To face the problem TIR images suffering from such a cold spatial average effect have been automatically identified and excluded from the computation of reference fields. In order to identify them the values of the temporal average μ_T of $T(t)$ and its standard deviation σ_T have been computed (using all the dataset of SEVIRI images collected over Greece in between May 2004 and December 2013) and for those scenes having $T(t) < \mu_T - 2\sigma_T$ [being $T(t)$, μ_T and σ_T all computed separately for land or sea pixels] the corresponding land (or sea) portions of image have been excluded from reference field computation.

Furthermore, even if not producing a cold spatial average effect, an extended cloud coverage can determine values of $T(t)$ and then of the considered signal $\Delta T(x,y,t)$ scarcely representative of the actual conditions of cloud-free pixels. So, when the cloudy fraction of land (or sea) portion of the scene was $>80\%$, then that portion (i.e., all pixels belonging to that land or sea class) have been excluded from the computation of the reference fields $\mu_{\Delta T}(x,y)$ and $\sigma_{\Delta T}(x,y)$.

Owing to these improvements, more reliable $\mu_{\Delta T}(x,y)$ and $\sigma_{\Delta T}(x,y)$ reference fields than the ones achievable using the standard RST pre-processing phases, have been finally computed (Fig. 2.1). In Figure 2.2 it is shown, separately for land and sea classes, the day-by-day results of the analysis performed on the whole data set of TIR images. RETIRA indexes $\Delta T(x,y,t)$ have been then computed for all MSG-SEVIRI TIR images belonging to the dataset producing one Thermal Anomaly Map (TAM) for each day t in between May 1st 2004 and December 31st 2013. Locations with $\otimes \Delta T(x,y,t) \geq 4$ (i.e., with signal excess $\Delta T(x,y,t) - \mu_{\Delta T}(x,y) \geq 4\sigma_{\Delta T}(x,y)$) will be particularly addressed and referred as Thermal Anomalies (TAs).

The particular spatial distribution of this kind of TAs and their transitory character in the temporal domain normally can allow to identify those possibly related to an impending Earthquake.

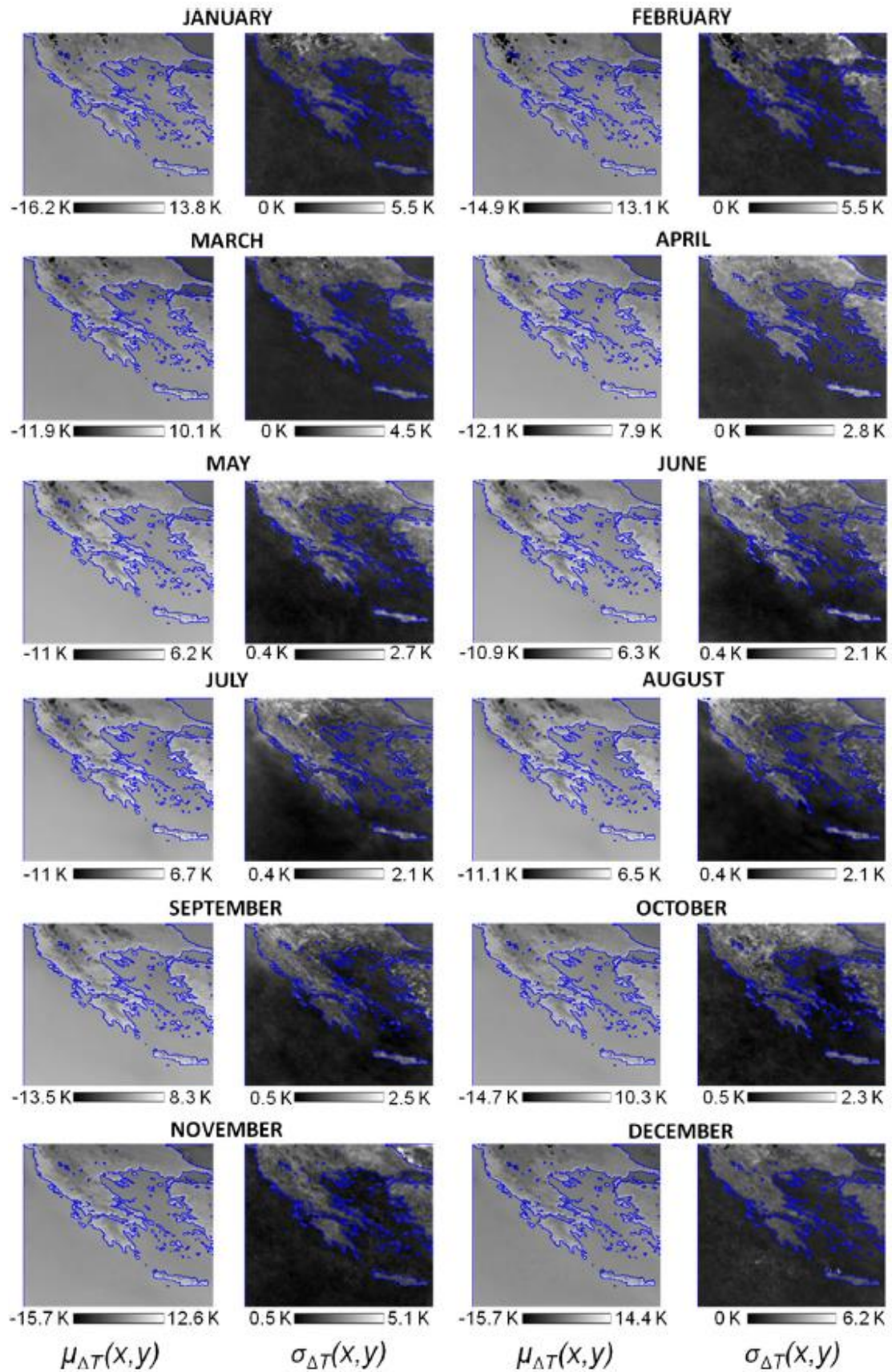


Figure 2. 1 Monthly reference fields $\mu_{\Delta T}(x,y)$ and $\sigma_{\Delta T}(x,y)$ computed for all the months of the year on the basis of SEVIRI TIR observations acquired over Greece from May 2004 to December 2013 (Eleftheriou et al., 2015).

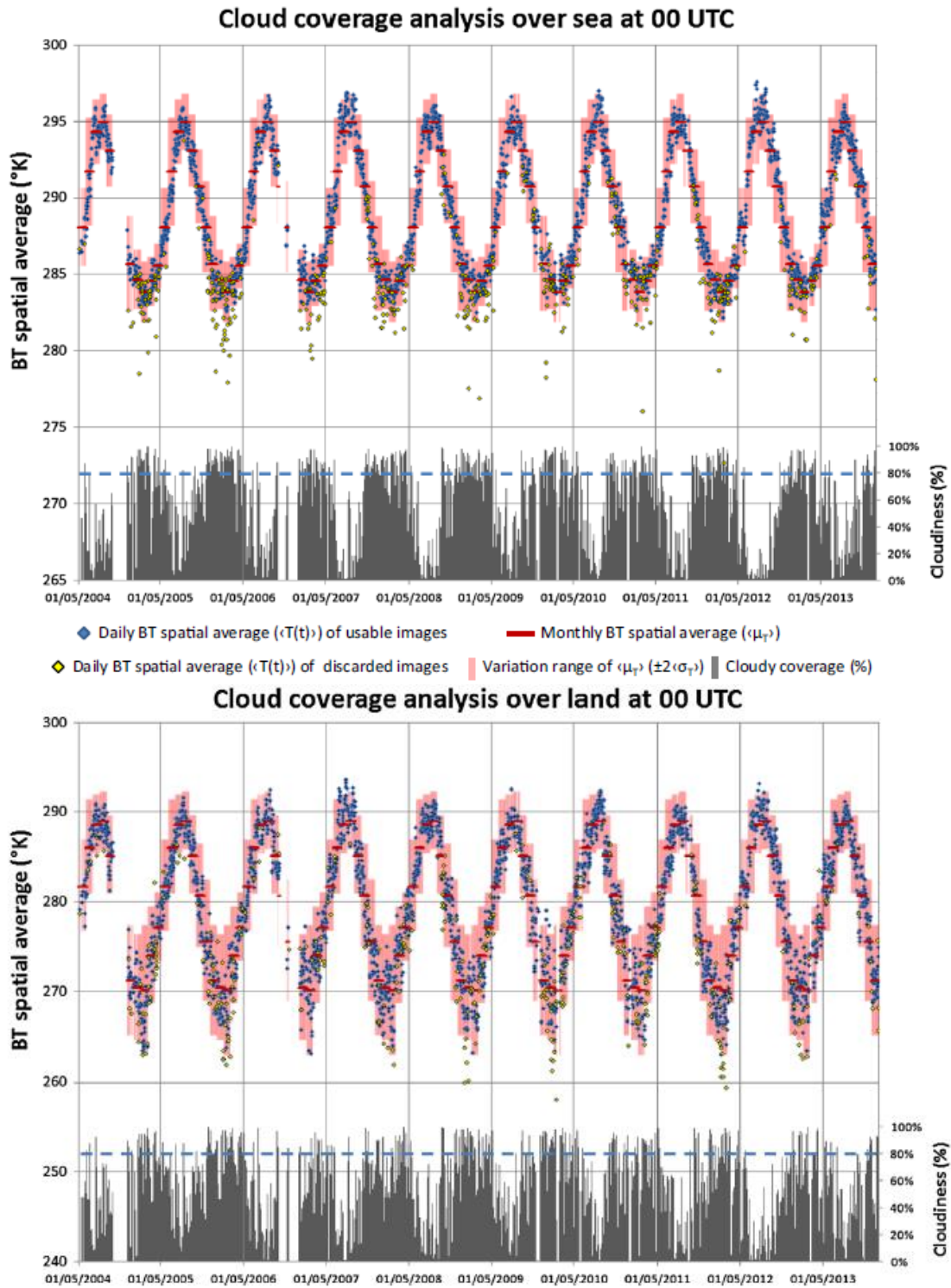


Figure 2. 2 Each rhomb represents the spatial average $T(t)$ computed on a TIR image collected over Greece on the day t at 00:00 UTC considering only cloud-free pixels. Blue rhombs correspond to scenes used for the computation of reference fields, the yellow ones to scenes removed from the used data sets. Red lines and light red bands represent, respectively the temporal averages $\langle \mu_T \rangle$ and ± 2 sigma bounds $(2\langle \sigma_T \rangle)$ computed considering the images collected during the same month in the past. Vertical gray bars represent the percentage of cloudy pixels identified over each scene. The dashed horizontal blue line indicates the cloudiness limit of 80% adopted to exclude cloudy scenes from reference field computation.

This is the reason why (together with relative intensity) spatial extension and persistence in time are requirements to be satisfied in order to preliminarily identify what we call significant thermal anomalies (STAs). Like in all the previous applications to thermal monitoring of Earthquake prone area (Aliano et al., 2007a, b, 2008a, b, c, 2009; Bonfanti et al., 2012; Corrado et al., 2005; Di Bello et al., 2004; Filizzola et al., 2004; Genzano et al., 2007, 2009a, b, 2010, 2015; Lisi et al., 2010; Pergola et al., 2010; Pulinets et al., 2007; Tramutoli et al., 2001, 2005, 2009, 2012a, b, 2013a, b, 2015b) TA highlighted by RST methodology have been subjected to such a preliminary space–time persistence analysis before they were qualified as STAs. However, other well-known (see for instance Filizzola et al., 2004; Aliano et al., 2008a; Genzano et al., 2009a) spurious effects exist that prevent to include among STAs some, even space–time persistent, sequence of TAs. The ones already identified are:

- TAs due to meteorological effects (Figure 2.3)

As above mentioned, these are all anomalous pixels appearing in the TIR scenes affected by a wide cloudy cover or in the TIR scenes affected by an asymmetrical distribution of clouds mainly over the warmest portions of a scene, which expose the remaining clear portions of the scene to the appearance of spurious anomalies (cold spatial average effect, Aliano et al., 2008a; Genzano et al., 2009a). Such a circumstance could appear in the portions of TIR scene having the daily spatial average $\langle T(t) \rangle \leq \langle \mu_T \rangle - \langle \sigma_T \rangle$ (being $\langle \mu_T \rangle$ and $\langle \sigma_T \rangle$ the monthly average and corresponding standard deviation of $T(t)$ computed for the same month of the image at hand using the whole historical dataset of TIR images) or having a cloudy coverage ≥ 80 % of total pixels of the same classes (land/sea). Moreover, also TAs generated by local warming due to night-time cloud passages have been recognized as artifacts of the meteorological effects (see Aliano et al., 2008a).

- TAs due to errors in image navigation/co-location process (Figure 2.3)

Although, this artifact is not rare for polar platforms, also in the cases of geostationary platforms a wrong navigation may cause intense TAs where sea pixels turn out to be erroneously co-located over land portions (see Filizzola et al., 2004; Aliano et al., 2008b).

- Space–time persistent TAs due to extreme events
Usually, these TAs can be observed in relation with particularly rare (over decades) events increasing (for more than 1 day) measured TIR signal because of an increase of surface temperature (e.g., in the case of extremely extended forest fires) or emissivity (e.g., extremely extended floods).

Taking into account these considerations an operational definition of STA can be given by considering a location x, y affected by a STA at the time t if the following requirements are satisfied:

- Relative intensity $\otimes_{\Delta T}(x,y,t) > K$ (with $K = 4$ in our case)
- Control on spurious effects. Absence of known sources of spurious TAs (see above)
- Spatial persistence. It is not isolated being part of a group of TAs covering at least 150 km^2 within an area of $1^\circ \times 1^\circ$
- Temporal persistence. Previous conditions (i.e. the existence of a group of TAs covering at least 150 km^2 within an area of $1^\circ \times 1^\circ$ around x, y) are satisfied at least one more time in the ± 7 days temporal window around t .

After applying the above-mentioned rules to the whole data set of 3151 SEVIRI scenes over Greece, 62 Significant Sequences of Thermal Anomalies (SSTAs) were identified where each one is composed by several STAs spanned on 2 or more TAMs.

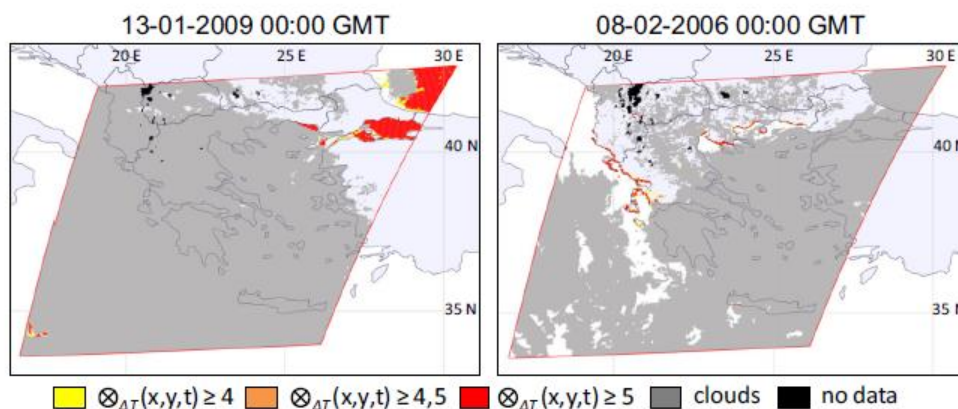


Figure 2. 3 Left side an example of artifacts due to the cold spatial average effect (see text) in the SEVIRI TIR image of the 13 January 2009 at 00:00 GMT. Right side an example of artifacts due to navigation/co-location errors in the processing of SEVIRI TIR image of the 8 February 2006 at 00:00 GMT.

2.1.1 Correlation analysis with seismic events with $M > 4$

In order to evaluate the possible correlations existing among the appearance of SSTAs and time, location and magnitude of Earthquakes, empirical rules were applied. They are mostly based on the long-term (more than 14 years) experience on TAM analyses (Aliano et al. 2007a, b, 2008a, b, c, 2009; Bonfanti et al. 2012; Corrado et al. 2005; Di Bello et al. 2004; Filizzola et al. 2004; Genzano et al. 2007, 2009a, b, 2010, 2015; Lisi et al. 2010; Pergola et al. 2010; Pulinets et al. 2007; Tramutoli et al. 2001, 2005, 2009, 2012a, b, 2013a, 2015b) performed by various authors in four different continents, different tectonic settings, for tens of Earthquakes with magnitudes ranging from 4.0 to 7.9. Each single STA observed at the time t in the location (x,y) will be considered possibly related to seismic activity if:

- It belongs to a previously identified SSTA;
- An earthquake of $M \geq 4$ occurs 30 days after its appearance or within 15 days before (temporal window);
- An Earthquake with $M \geq 4$ occurs within a distance D , from the considered STA, so that $150 \text{ km} \leq D \leq R_D$ being $R_D = 10^{0.43M}$ the Dobrovolsky et al., (1979) distance (spatial window).

Hence, starting from each STA belonging to an SSTA, different possibly affected areas can be built for different possible magnitudes of future/past Earthquakes. The convolution of the contours drawn for all the STAs belonging to the same SSTA, allow to draw the contours of the areas (different for different magnitudes) possibly affected by future/past Earthquakes. The possible correlation among previously identified SSTAs and Earthquake occurrence was investigated considering all Earthquakes⁵ with magnitude $M \geq 4$ occurred from April 1st 2004 to January 31st 2014 in:

- The area (contoured in red in figure 2.3) of TAMs (top-left 42.1°N—19.2°E; top-right 42.7°N— 30.4°E; bottom-right 33.9°N—26.1°E; bottom-left 33.5°N—16.7°E) using the seismic catalog of National Observatory of Athens (NOA 2014) for the Greek territory

⁵ 1083 events with $M \geq 4$, 80 events with $M \geq 5$ and 8 events with $M \geq 6$.

- The area extending up to 1° from its borders (top left 43.1°N—18.2°E; top-right 43.7°N—31.04°E; bottom-right 32.9°N—27.1°E; bottom-left 32.5°N—15.7°E) using the seismic catalog of National Earthquake Information Center of U.S Geological Survey (USGS 2014).

The analysis performed by applying previously established correlation rules to all the 62 SSTAs identified on the whole time series of SEVIRI TIR observations in the period May 2004 to December 2013 highlighted 58 SSTAs (~93 % of the 62 previously identified) in apparent space–time relations with Earthquake occurrence and only 4 SSTAs (~7 %) apparently not related to documented seismic activity.

2.1.2 Correlation analysis by using a barycentral approach

The analysis performed using a barycentral approach was used in order to reduce the alarm area, in an attempt to better define the whereabouts of the future Earthquake epicenters. By means of this, the barycenter of all the previous mentioned 62 SSTAs was calculated and a new ‘buffer zone’ (using the Dobrovolsky et al., (1979) distance spatial window) around that point was created. The calculation of the barycenter was done by using ArcGIS Desktop, by the spatial statistics tool ‘Central Feature’ that identifies the most centrally located feature in a point, line, or polygon feature class, which, in the case of the SSTAs identifies the most centrally located polygon in respect also to its RETIRA value (Figure 2.4).

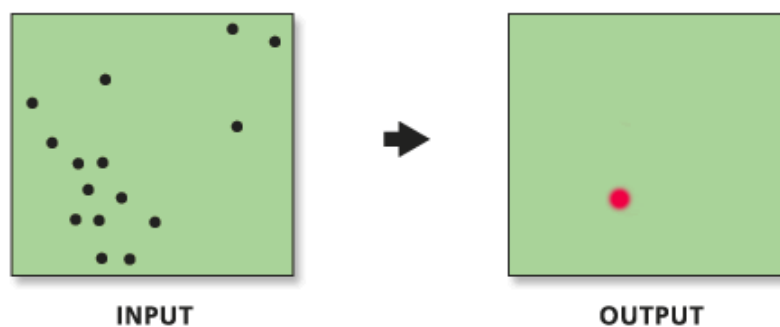


Figure 2. 4 The feature associated with the smallest accumulated distance to all other features is the most centrally located feature, weighted also by its value (the RETIRA index value) (Taken from http://resources.esri.com/help/9.3/arcgisengine/java/gp_toolref/spatial_statistics_tools/central_feature_spatial_statistics_.htm).

The application of the barycentral approach on the previously established correlation rules to all the 62 SSTAs identified on the whole time series of SEVIRI TIR observations in the period May 2004 to December 2013, highlighted 46 SSTAs (~75 % of the 62 previously identified) in apparent space–time relations with Earthquake occurrence and 16 SSTAs (~25 %) apparently not related to documented seismic activity. This approach gives a more precise area to expect the impending Earthquake but reduces the total number of the correlated seismicity. An example can be seen in Figure 2.5, where, on the left image, the alarm area (pink zone) represents a distance of 150 km from each pixel (blue) of the merged⁶ SSTAs observed on 23, 24 and 25 January 2007, which in this case includes a seismic event (green star) occurred on 23 January 2007 with M=4.9. Instead, the image on the right, shows that with the barycenter approach (red circle), the same seismic event is not included in the first buffer zone (150km radius). The results of the barycentral approach will be discussed in detail in the following, while a total view of the analysis can be seen in Figure 2.6.

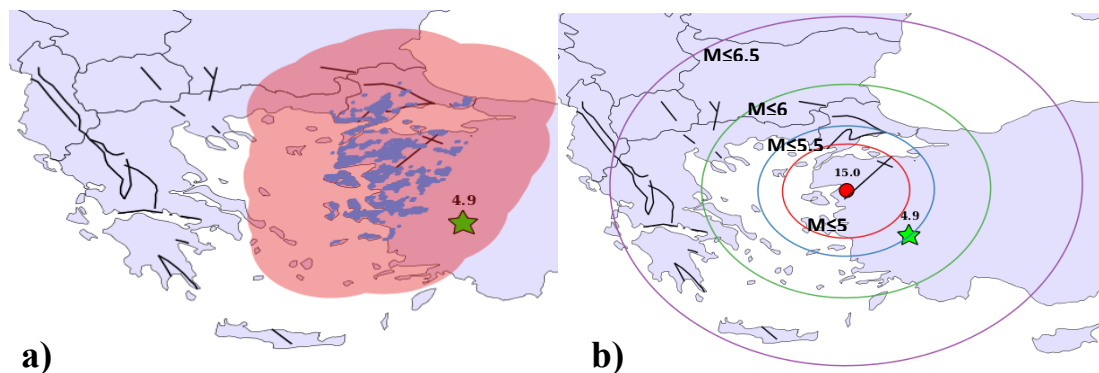


Figure 2. 5 a) Buffer zone (depicted in pink) represents an alarm area with a radius of 150km from each thermal anomalous pixel (blue) and the seismic event (green star) follows the space-time correlation rules. b) The red spot represents the barycenter of the thermal anomalies and the consecutive circles around it the buffer zones following the Dobrovolsky et al., (1979) distance law. It is visible that the seismic event (green star) doesn't follow the space correlation rule and is not included in the first buffer zone (red circle).

⁶ The thermal anomalous pixels of each day of the sequence that are in $1^{\circ} \times 1^{\circ}$ spatial relation are merged in order to have one shapefile and calculate a unique barycenter for each SSTAs.

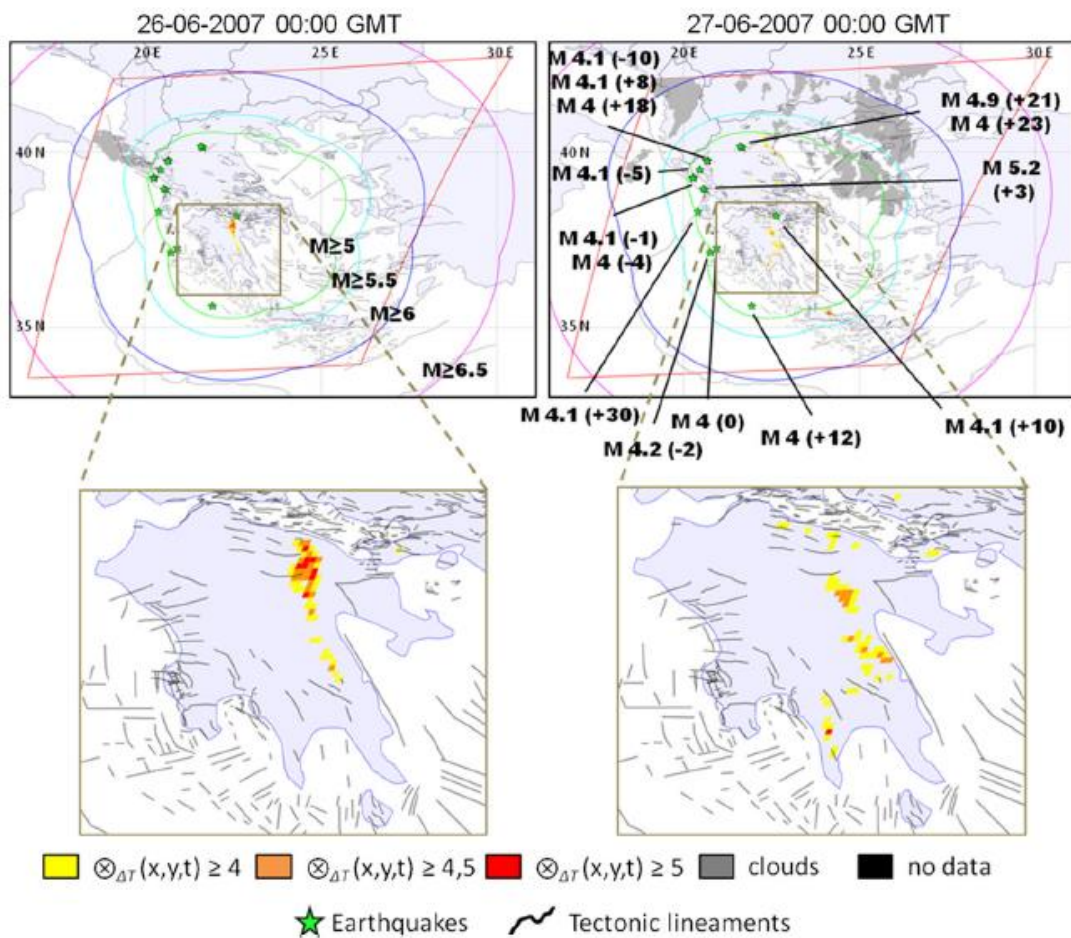
Figure 2. 6 Correlation analysis among Thermal Anomalies and Earthquakes with $M \geq 4$ occurred over Greece from May 2004 until December 2013 (see text). All 62 identified SSTAs have been reported one per each row (affected area and actual start date are reported on the left). The cells corresponding to the day of the first STA is reported in yellow (in correspondence to the day zero) each following persistence is depicted in red. Black and gray cells indicate, respectively, the absence of available satellite data and days with a wide cloud coverage (not usable data) in the investigated area. Cells with numbers indicate days of occurrence, and magnitude, of seismic events (asterisk indicates that the maximum magnitude is reported in the case of more than one event per day). For each SSTA the considered period (i.e., 30 days after last STA and 15 days before the first STA) is bounded by a black line. The 16 SSTAs apparently not associated with Earthquakes are depicted in orange.

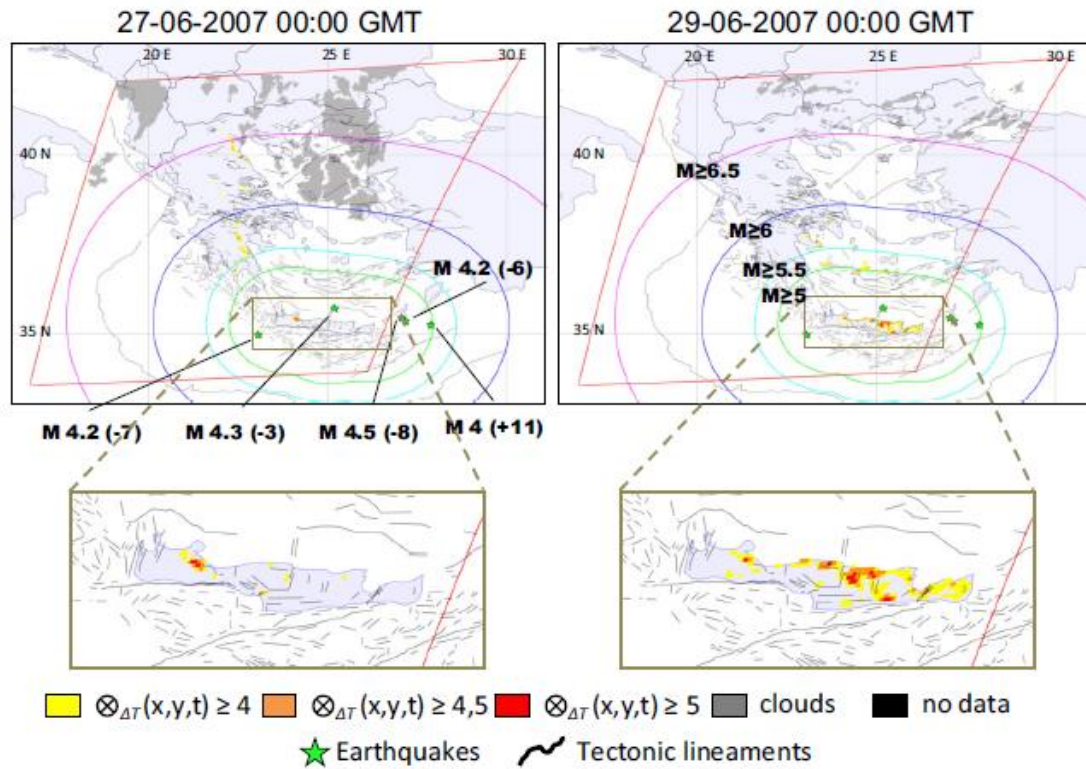
2.1.3 Analysis of results

At first glance it is noticeable that most of identified STAs appear few days around the time of the Earthquake and are generally localized near main tectonic lineaments of the epicentral area (Eleftheriou et al., 2015). Looking for instance at the example shown in Figure 2.7 it is possible to note, in the period 26–29 June 2007, the presence of two different SSTAs:

- Peloponnesus region (upper part of Figure 2.7): several STAs appear near tectonic lineaments from June 26th, up to June 29th, 2007. A seismic event with $M = 5.2$ occurred on 29 June 2007 (3 days after the first STA appearance) and various other with $M \geq 4$ (before and after the first STA appearance), all well within the corresponding spatial correlation windows.
- Crete island (bottom part of Figure 2.7): STAs appear in the western part of the island on 27 June 2007 and, with a greater spatial extension, on 29 June 2007 in the eastern part just few days after the occurrence of several low magnitude Earthquakes (i.e., from 4.2 to 4.5) in the Sea of Crete.

Figure 2. 7 Examples of SSTAs identified in the period 26–29 June 2007. Significant TAs (STAs) with $\otimes_{\Delta T}(r,t) \geq 4$ (depicted in different colors according to the corresponding RETIRA values) appear in the Peloponnesus area on 26 and 27 June 2007 (upper part) and in Crete island on 27 and 29 June 2007 (bottom part) before and after $M \geq 4$ seismic events. In addition to the magnitude of Earthquakes, also the temporal gap from the first appearance of STAs is indicated by a number (N) in parentheses ($\pm N$ means that the Earthquake occurred N days after/before the first appearance of STAs). Contours in different colors correspond to different space/magnitude windows (Dobrovolsky et al., 1979). The red contoured box indicates the limits of analyzed SEVIRI TIR scenes (Thermal Anomaly Map area).





As foreseen by general (e.g., Scholz et al., 1973) and specific (Tramutoli et al., 2013a) physical models, SSTAs appear mostly before but also after the occurrence of seismic events, showing however an increasing tendency to appear mostly before (more than 66 % of the total) in the cases of medium–high magnitude Earthquakes ($M \geq 5$). Regarding the previous analysis, in figure 2.8, the Distribution of the SSTAs with respect to the Earthquake occurrence can be seen.

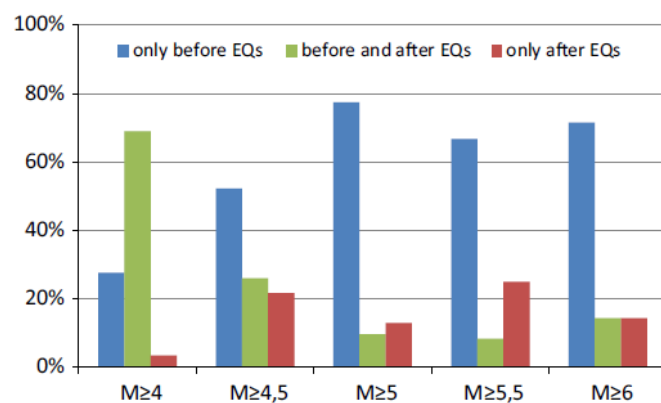


Figure 2. 8 Distribution of the SSTAs with respect to the Earthquake occurrence for different class of magnitude.

The barycentral analysis revealed a more precise alarm area (Figure 2.9). It is important to mention that in some cases the spatial window rule is not fulfilled just for a few kilometers (i.e. $\pm 20\text{km}$) away from the barycenter, resulting in missing the identification of strong events (Figure 2.10). A closer view on the results of the two analyses (normal and barycentral) shows that in the first case, there were 235 seismic events with $M \geq 4$ associable to the 58 SSTAs out of which, 158 (i.e. 67%) Earthquakes occurred after the observed SSTAs and 77 (i.e. 33%) Earthquakes occurred before the observed SSTAs. Instead, in the case of the barycentral approach, there were 117 seismic events with $M \geq 4$ associable to the 46 SSTAs out of which, 79 (i.e. 67.5%) Earthquakes occurred after the observed SSTAs and 38 (i.e. 32.5%) Earthquakes occurred before the observed SSTAs.

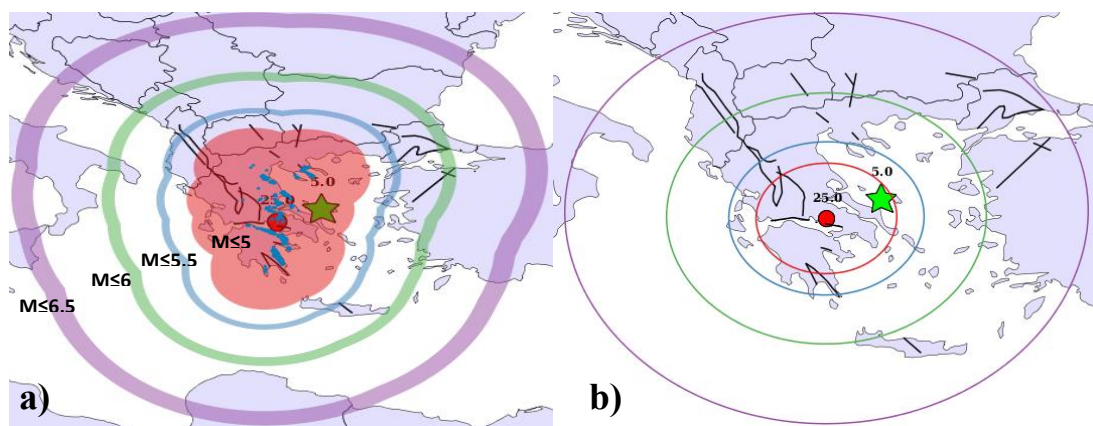


Figure 2. 9 a) Merged thermal anomalies (blue) observed on 18 and 19 March 2008. b) Visualization of the barycenter (red spot), and the alarm area (colorful circles), for the seismic event (green star; $M=5.0$), occurred on 19 March 2008. The more precise alarm area fulfills the spatial correlation rules.

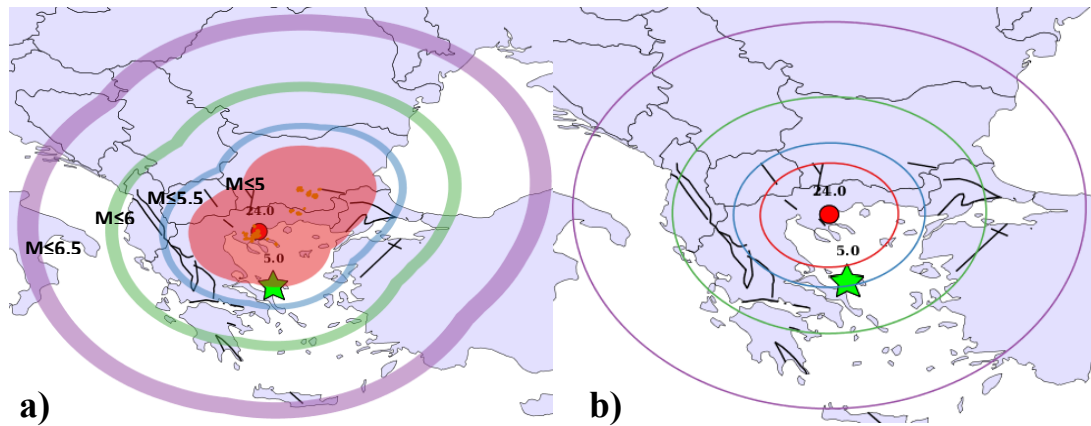


Figure 2.10 a) Merged thermal anomalies (orange) observed on 24, 27 and 28 February 2008. b) Visualization of the barycenter (red spot), and the alarm area (colorful circles), of the seismic event (green star; $M=5.0$), occurred on 19 March 2008. The barycentral alarm area does not fulfill the spatial correlation rules.

On a closer view to the 46 SSTAs associable to Earthquakes with $M \geq 4$, it is possible to note that:

- 15 (~33%) SSTAs occurred before and after the seismic events (PRE-POST seismic SSTAs);
- 22 (~47%) SSTAs occurred only before the seismic events (PRE seismic SSTAs);
- 9 (~20%) SSTAs occurred only after the seismic events (POST seismic SSTAs)

The distribution of the 62 SSTAs barycenters over Greece can be seen in Figure 2.11. To better understand the areas where thermal anomalies are mostly observed and their relation with seismic activity, a comparison with seismotectonic features can be done. For example, looking the distribution of the barycenters and the active faults of the broader Aegean Region (Figure 2.12), it is visible that thermal anomalies mostly appear near the individual seismogenic sources (ISSs) (see legend of the figure). In particular, most of them are around Peloponnesus, central and north Greece but also near the composite seismogenic sources (CSSs), over and around Crete Island. The study area was separated in five zones regarding the appearance of thermal anomalies (barycenters). The percentage of success of each area can be seen in Table 2.1. It is worth mentioning that the largest number of SSTAs is observed around the zone Ionian

– Peloponnesus – Central Greece, with a percentage of success (~80%). Taking into account also the Seismic density map (Figure 2.13, analyzed using ZMAP software), it is possible to conclude that the areas with higher possibility of a strong Earthquake occurrence are mostly near the observed thermal anomalies. The map in Figure 2.14 shows 17 strong Earthquakes ($M \geq 5$) occurred in the investigated period/areas preceded or followed by SSTAs in the prescribed space-time correlation window), confirming the above cited correlation.

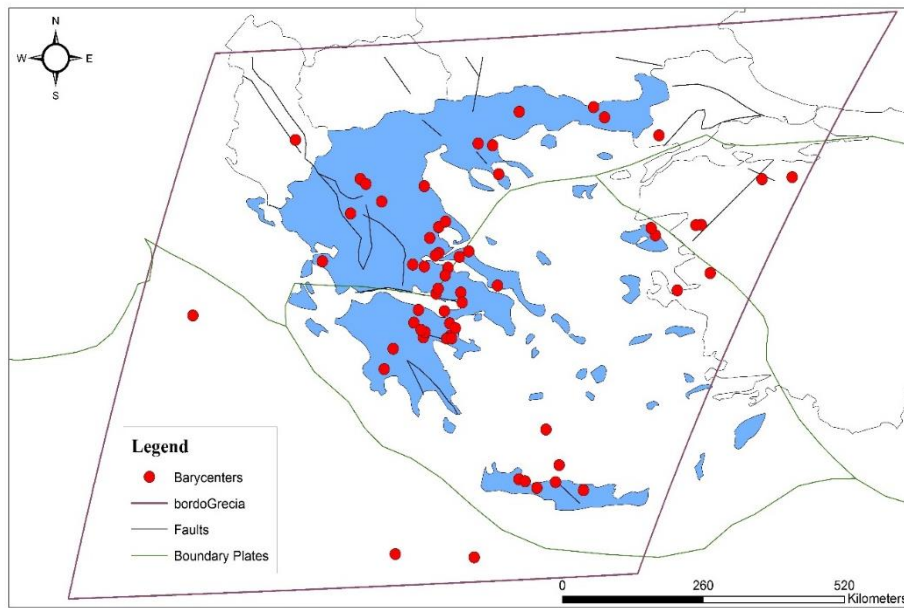


Figure 2. 11 Distribution of the 62 SSTAs barycenters over Greece. The barycenters are depicted in red, the borders of the area analyzed are in purple, main faults are indicated with blue lines and the boundary of the tectonic plates with green lines.

Zone	Total Number of SSTAs	Positive	False Positive	Percentage of Success
Crete - Mediterranean - Aegean	9	6	3	66,67
Ionian - Peloponnese - Central	29	23	6	79,31
Epirus - Thessalia	9	7	2	77,78
Makedonia - Thraki	6	3	3	50,00
Dodecanese - Turkey	9	7	2	77,78

Table 2. 1 Different Zones where thermal anomalies were observed and the percentage of success.



Figure 2. 12 Active Faults of the broader Aegean Region
(<http://gredass.unife.it/>)

LEGEND

Earthquakes (M = Magnitude): 550 BC - 2010 AD (Papazachos et al., 2000; 2010)



$M \geq 7.0$



$6.0 \leq M < 7.0$



$5.5 \leq M < 6.0$

Individual Seismogenic Sources: they are obtained from geological and geophysical data and are characterized by a full set of geometric (strike, dip, length, width and depth), kinematic (rake, average displacement per event) and seismological (magnitude, slip rate, return period) parameters. ISSs are assumed to exhibit "characteristic" behaviour with respect to rupture length/width and expected mean and maximum magnitude. Moreover, ISSs can also be considered as fault segments of larger fault zones when there are evidences of individual rupture. The ISSs favour accuracy of the information supplied over the completeness of the sources themselves. As such, they can be used for deterministic assessment of seismic hazard, for calculating earthquake and tsunami scenarios, and for tectonic and geodynamic investigations.

Composite Seismogenic Sources: they are obtained from geological and geophysical data and characterized by geometric (strike, dip, width, min/max depth) and kinematic (rake) parameters, but their sliding surface geometry is more loosely defined and can contain an unspecified number of ISSs. They are not assumed to be capable of a characteristic earthquake but their potential can derive from existing earthquake catalogues or other geological considerations. A CSS is essentially inferred on the basis of regional surface and subsurface geological data that are exploited well beyond the simple identification of active faults or youthful tectonic features. Opposite to the ISSs, this category of sources favours completeness of the record of potential earthquake sources over accuracy of source description. In conjunction with seismicity and modern strain data, CSSs can thus be used for regional probabilistic Seismic Hazard Assessment and for investigating large-scale geodynamic processes. A CSS can represent a large fault zone which can consist of one or more well defined ISSs. However, it can also be 'empty' of ISSs if none can be recognized. The seismic behaviour of the CSSs can be completely independent for the ISSs, given that a potential event may rupture the total length of the source, whether it contains none, one or more ISSs.

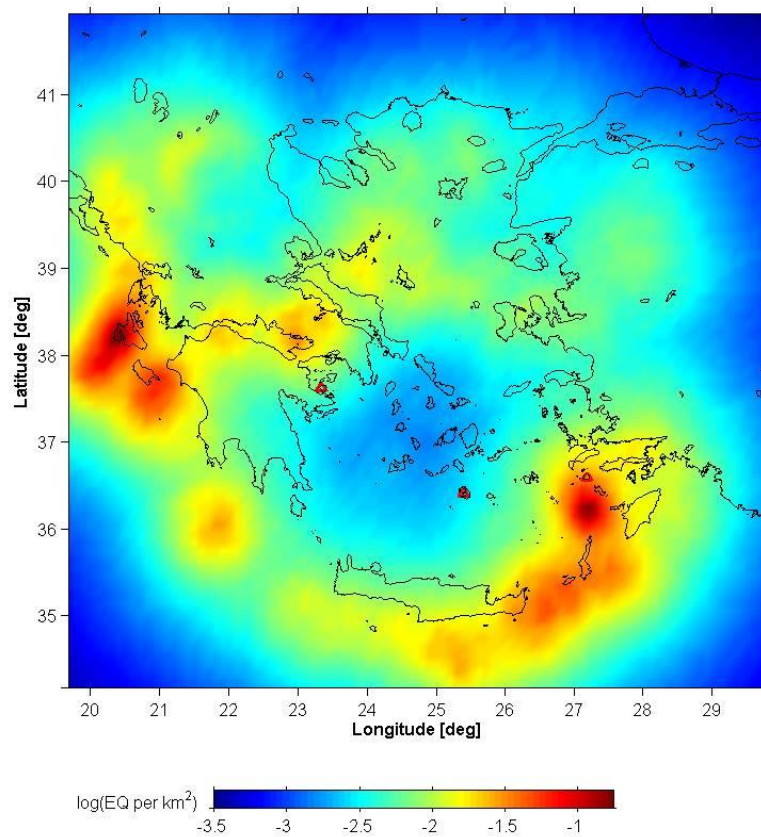


Figure 2. 13 Seismic density map. The catalog used for this analysis was taken from the National Observatory of Athens (NOA), and includes all the seismic events with $M \geq 4$ that occurred in the period between January 1980 until May 2016 in Greece.

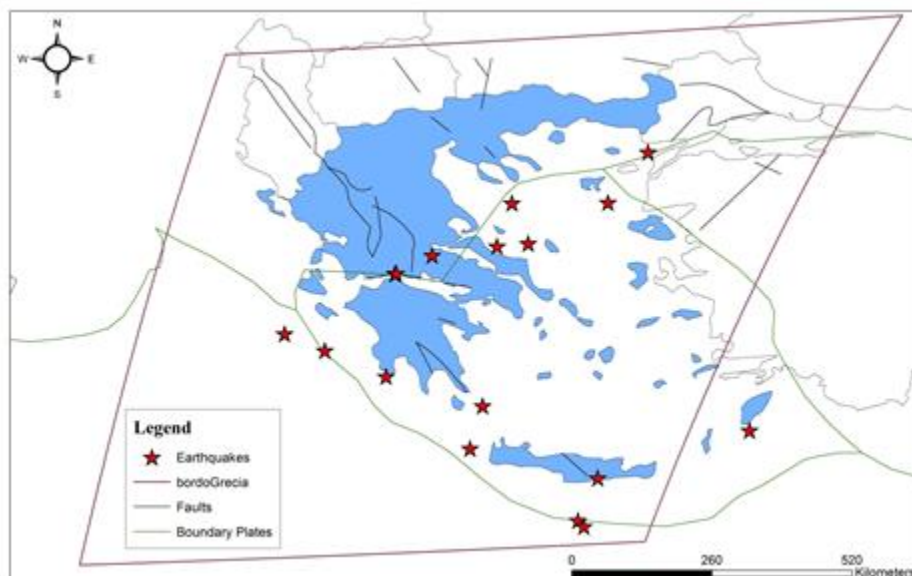
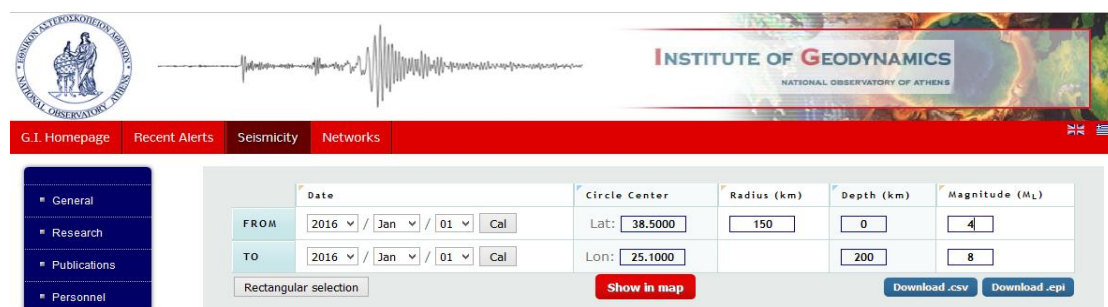


Figure 2. 14 Seventeen Earthquakes ($M \geq 5$) (red star) related to the SSTAs. 13 events occurred after the observation of SSTAs and 4 events before.

2.2 Long-term NTA analysis of seismic data over Greece (NTA)

As seen in the first chapter, by applying natural time analysis in time series of Earthquakes, it is possible to see if the system enters in a critical state a few days or weeks before strong seismic events. A long-term natural time analysis was performed in this study. In particular, for each of the 62 SSTAs, Earthquake catalogs was generated using the tool of the National Observatory of Athens (Figure 2.15) centered on the barycenter of each SSTAs, with a buffer zone (radius) of 150 km and magnitude of completeness $M=2.2$. Two kinds of catalogs were produced for each of the SSTAs, making in total 124 Earthquake catalogs, 62 out of which have a starting date fifteen days before the first STAs and 62 that has a starting date on the same date of the first STAs. The study was performed in this way in order to better understand which of the two analyses will provide a better starting point for NTA of seismicity related to the aforementioned SSTAs. It is worth noting that it is centered on the barycenter for selecting seismic data without knowing future epicenters. In this manner, this analysis may provide information for the correlation of the two methodologies in order to move to a real-time analysis.



	Date	Circle Center	Radius (km)	Depth (km)	Magnitude (M _L)
FROM	2016 / Jan / 01	Lat: 38.5000	150	0	4
TO	2016 / Jan / 01	Lon: 25.1000		200	8

*Figure 2. 15 Search engine for Earthquake catalogs
(<http://www.gein.noa.gr/en/seismicity/maps> (2016))*

2.2.1 Correlation analysis with strong seismic events

All the 124 Earthquake catalogs were fixed properly in Microsoft Excel in order to have the right format and be ready to be analyzed using MATLAB with specified scripts following the prescriptions of NTA. The results of the analysis are as described in the following.

Having as a starting point of the Earthquake catalogs equal to fifteen days prior the date of the first STAs, 12 strong events with $M \geq 5$ (all of them defined as POST-seismic, namely, occurred some days or weeks after the STAs) were analyzed. NTA showed critical points from a few hours up to 27 days prior to 9 (~75%) of the strong events (Table 2.2). A closer view on the results of Table 2.2, shows that NTA critical point can be expected up to 2 weeks before/after the first day of STAs observations. It is worth mentioning the case of the SSTAs on 16/12/2005 and 3/1/2006 which are related to the same Earthquake occurred on 8/1/2006 ($M=6.4$) but the critical point from the NTA is appeared only on the first. The distance between the Earthquake epicenter and the barycenter of the two SSTAs can be seen on the Table 2.2. This might give information to better understand (always with relation with other parameters, i.e. geotectonic, geological) the preparation phase/area of the impending Earthquakes.

Table 2. 2 Results of NTA on the seismicity prior to strong Earthquakes that thermal anomalies were preceded. Orange color indicates the events for which no critical point was determined and blue color indicates the cases where the critical point appeared before the SSTAs.

First day of Observation	Date of related Earthquake	Magnitude	Date of NTA critical point	EQ-NTA	EQ-TIR	NTA-TIR	Distance from Barycenter (km)
14/1/2005	31/1/2005	5,7	-	-	17	-	264
16/12/2005	8/1/2006	6,4	24/12/2005	15	23	8	186
3/1/2006	8/1/2006	6,4	-	-	5	-	490
18/3/2008	19/3/2008	5	19/3/2008	0	1	1	132
9/7/2008	15/7/2008	6,4	12/7/2008	3	6	3	536
4/12/2008	13/12/2008	5,2	29/11/2008	14	9	-5	67
1/1/2010	18/1/2010	5,2	8/1/2010	10	17	7	56
25/2/2010	9/3/2010	5,1	10/2/2010	27	12	-15	155,6
27/5/2013	15/6/2013	5,8	19/5/2013	27	19	-8	141
27/5/2013	6/6/2013	5	6/6/2013	0	10	10	52,9
2/10/2013	12/10/2013	6,2	20/9/2013	22	10	-12	261
13/12/2005	8/1/2006	6,4	-	-	26	-	221

A similar analysis was done on the other Earthquake catalogs, namely, the ones having as starting date the same as the first day of observation of SSTAs. As mentioned above, the NTA was performed on the 12 strong events with $M \geq 5$. The analysis can be seen in Table 2.3. Critical points were seen prior to only 4 (~34%) out of the 12 seismic events. This can be due to the fact that few seismic events occurred before the main shocks when starting the catalogs the same day of the SSTAs observation. As a result, not

having enough time series of Earthquakes to be analyzed in natural time and properly follow the evolution of the seismicity before the strong events.

Table 2. 3 Results of NTA on the seismicity prior to strong Earthquakes that thermal anomalies were preceded. Orange color indicates the events that there wasn't critical point.

First day of Observation	Date of related Earthquake	Magnitude	Date of NTA critical point	EQ-NTA	EQ-TIR	NTA-TIR	Distance from Barycenter (km)
14/1/2005	31/1/2005	5,7	29/1/2005	2	17	15	264
16/12/2005	8/1/2006	6,4	-	-	23	-	186
3/1/2006	8/1/2006	6,4	-	-	5	-	490
18/3/2008	19/3/2008	5	-	-	1	-	132
9/7/2008	15/7/2008	6,4	-	-	6	-	536
4/12/2008	13/12/2008	5,2	12/12/2008	1	9	8	67
1/1/2010	18/1/2010	5,2	-	-	17	-	56
25/2/2010	9/3/2010	5,1	25/2/2010	12	12	0	155,6
27/5/2013	15/6/2013	5,8	-	-	19	-	141
27/5/2013	6/6/2013	5	31/5/2013	6	10	4	52,9
2/10/2013	12/10/2013	6,2	-	-	10	-	261
13/12/2005	8/1/2006	6,4	-	-	26	-	221

Considering that the analysis of the Earthquake catalogs (15 days before the SSTAs) gave better results than the other one (same day as SSTAs), the NTA for the 9 strong events are reported in Annex 1, where, the Earthquake catalogs are plotted in the natural time domain and the other plots shows the relative power spectrum $\Pi(\varphi)$ according to the natural frequency φ .

2.2.2 Analysis of results

Natural time analysis was performed on all the 124 Earthquake catalogs of the 62 SSTAs, in order to have an overview of the critical points (i.e. positive and false-positive alarms) that appeared before the Earthquakes with $M \geq 4$ and are related to the SSTAs in the investigated area/period. The results can be seen in figures 2.16 and 2.17. In the first, there are 27 cases where we have a positive alarm and 9 cases giving a false-positive. Instead in the other figure, 19 cases showed a positive alarm and 9 false-positive. Regarding the two analyses on the Earthquake catalogs, the one, starting 15 days before the first day of observation of the STAs includes more seismic events occurred with $M \geq 2.2$ in the investigation area and hence gives more time to study the evolution of the seismicity in Natural time. However, there can be cases where there is

a strong seismic event a few days prior to the SSTAs (POST seismic SSTAs), and the Earthquake catalog can't be properly studied in natural time. These cases are considered as 'Occurrence of Earthquakes without critical point'. In the cases where there is only SSTAs (false-positive) they are considered as 'Neither Earthquake nor critical points'.

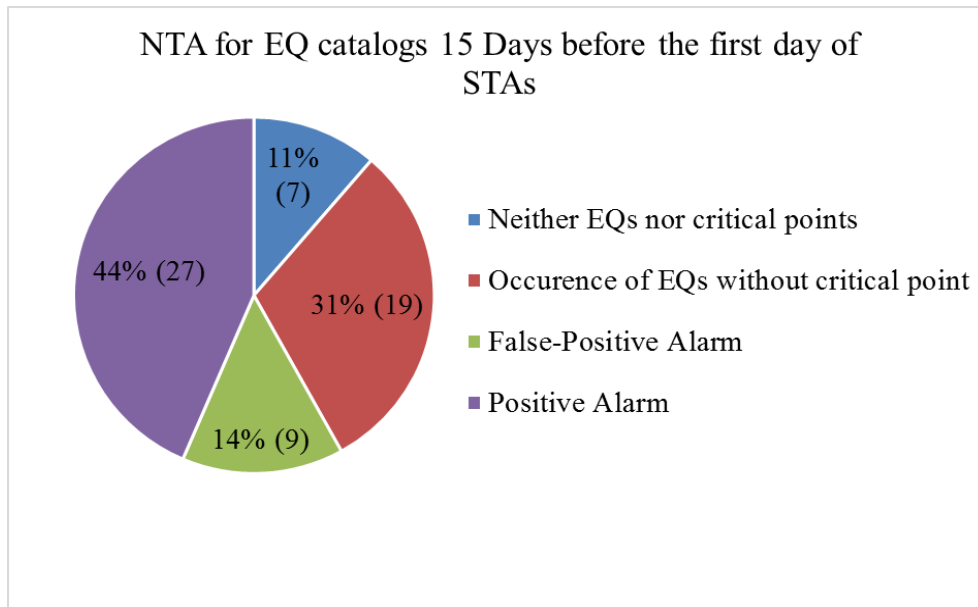


Figure 2. 16 NTA for EQ catalogs started 15 days before the first day of STAs

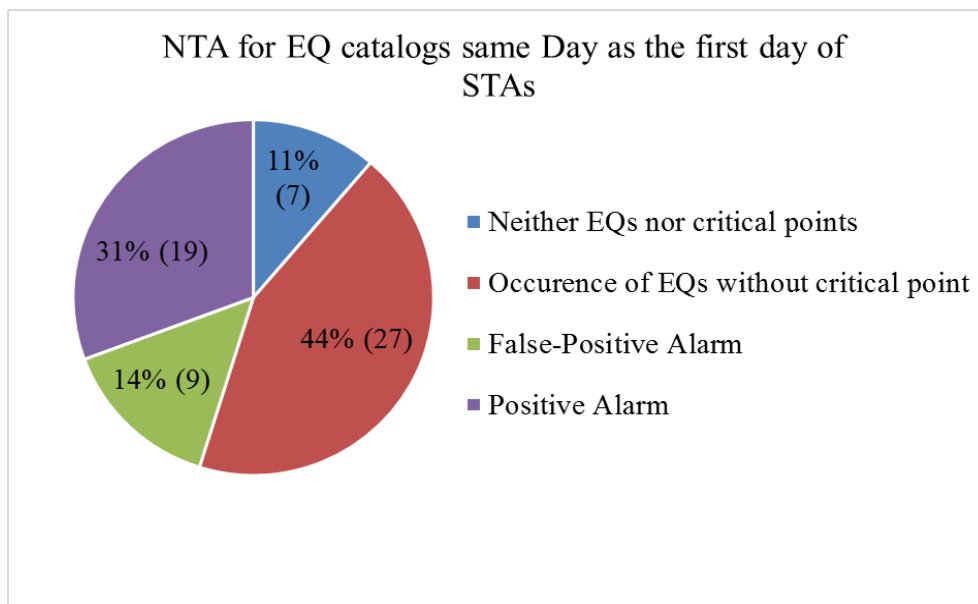


Figure 2. 17 NTA for EQ catalogs started the same day as the first day of STAs

The results of NTA in respect to the seismicity was discussed above. In the next chapter, the main results of this study, concerning the multi-parametric analysis of RST and NTA in respect to the seismicity preceded or followed by the STAs will be discussed in detail.

Chapter 3

Multi-parametric analysis

A multi-parametric analysis is important in order to fully understand the mechanisms of Earthquake preparation and their possible relation with other measurable quantities. The purpose of this chapter is to demonstrate if the results of the two methodologies are in correlation and can provide useful information for a possible Earthquake forecast.

3.1 Joint correlation analysis with seismic events ($M \geq 4$)

The natural time analysis was performed on the seismicity for all the 62 cases that SSTAs were observed. For this analysis, the Earthquakes with $M \geq 4$ that occurred 15 days prior and 30 days later than the first day of TAs, were studied. By applying NTA on the Earthquake catalogs before the identified seismic events ($M \geq 4$), the approach of the system to a critical stage can be seen in most of the cases and provide a more precise answer on which seismic events the precursors can be related to. Natural time analysis was performed on the seismicity that occurred around an area with a radius of 150 kilometers, centered on the barycenter of each SSTAs. An example can be seen in figure 3.1, where, the white spot in the center of the picture indicates the barycenter of the SSTAs whose first day of observation was on 18 March 2008. In the same figure the seismicity, which started on 3/3/2008 is depicted in colorful circles (see legend), the mainshock, occurred on 19 March 2008, is indicated by the yellow star and the red circle indicates the buffer zone (150 km radius). In that case, the NTA showed two times a critical point: the first appeared on 14/3/2008 and the second was on 19/3/2008, a few hours before the mainshock.

The results of the whole analysis will be discussed in detail in the following paragraph.

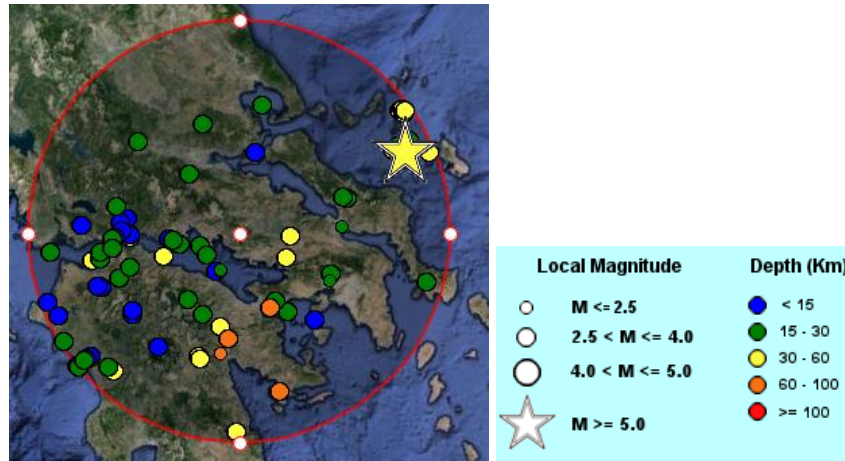


Figure 3. 1 Seismicity that occurred from 3/3/2008 until 19/3/2008 where a mainshock with $M=5.0$ took place. The study area is centered on the barycenter of the SSTAs (with a buffer zone 150 km) where the first observation was on 18/3/2008. The seismicity and the map is taken from the online tool of National Observatory of Athens (<http://www.gein.noa.gr/en/seismicity/maps> (2016)).

3.1.1 Analysis of results

The 62 SSTAs were divided in three classes in order to have a better understanding on the correlation analysis (Figure 3.2). The first class includes the SSTAs that were reported as Pre-Seismic SSTAs as well as Pre & Post-Seismic SSTAs. The second class includes only the SSTAs defined as Post-Seismic SSTAs and the third class includes the False-Positive SSTAs.

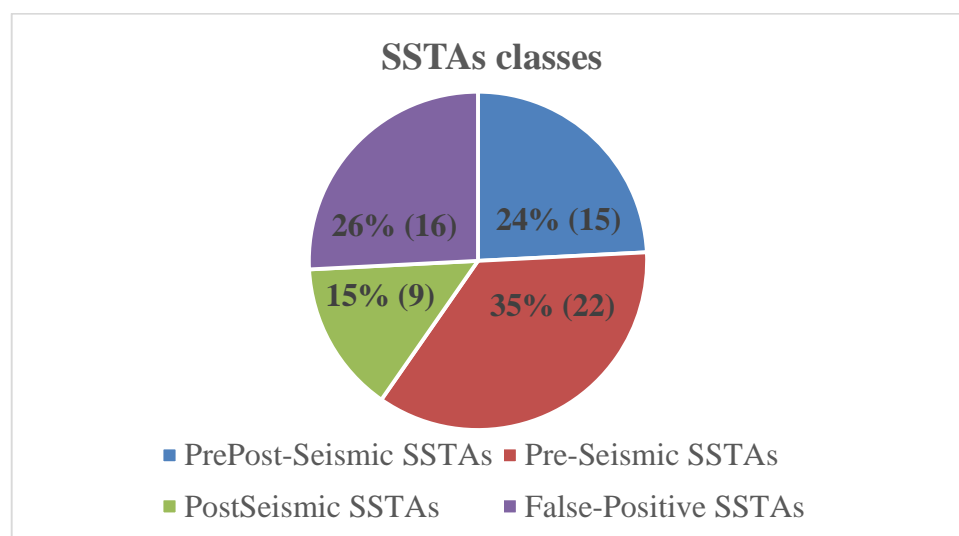


Figure 3. 2 SSTAs classes as defined in this study.

Concerning the analysis on the Earthquake catalogs that started fifteen days before the first day of observation of the SSTAs, in the 15 PrePost-Seismic SSTAs there are 10 (~67%) positive alarms that showed critical points, hence in correlation with natural time analysis, and 5 (~33%) for which there were both SSTAs and Earthquake occurrence but no critical point. Concerning the 10 positive alarms of critical points, there are 7 (70%) that appeared before the first day of observation of the SSTAs and 3 (30%) that appeared later. A closer view on the 7 cases that appeared before the first day of the SSTAs, shows that critical points appears in average up to 24 days and SSTAs up to 13 days prior to the seismic events.

Regarding the 9 Post-Seismic SSTAs, there are 3 (~34%) positive alarms that showed also critical points and 6 (~66%) for which there were SSTAs and Earthquake occurrence but no critical points. In the three cases where there are alarms from both the methodologies, NTA critical points appeared two times 1 day and one time 7 days prior to the seismic events. In the case of the 22 Pre-Seismic SSTAs, there are 14 (~64%) positive alarms that showed also critical points that there were observed from a few hours up to 28 days before the mainshock and 8 (~36%) for which there were SSTAs and Earthquake occurrence but no critical points. Lastly, in the 16 false-positive SSTAs, there are 9 (~57%) cases where there were critical points (false-positive) but no Earthquakes and 7 (~43%) cases where there were only SSTAs and neither Earthquake nor NTA critical points.

In total, focusing towards the multi-parametric results for a possible seismic hazard forecast, there are 73% positive alarms when putting together the results of the 10 PrePost and 14 Pre-Seismic SSTAs with the NTA and 27% false-positive that derives from the 9 NTA cases where there were critical points without the occurrence of Earthquakes.

Concerning the analysis on the Earthquake catalogs that started the same day as the first day of observation of the SSTAs, in the 15 PrePost-Seismic SSTAs there are 8 (~53%) positive alarms that showed critical points, hence in correlation with natural time analysis, and 7 (~47%) for which there were both SSTAs and Earthquake occurrence but no critical point. The analysis on the 8 positive alarms of critical points, shows that critical points appears in average up to 6 days after the SSTAs and up to 10 days prior

to the seismic events apart an exception that the critical point was observed after the mainshock.

In the 9 Post-Seismic SSTAs, the natural time analysis showed critical points in 3 cases, but they have to be considered false-positive alarms because in contrast with the model, they appeared after the occurrence of the main events ($M \geq 4$) and without a seismic event to follow in the space-time window. These cases are related with issue concerning the decision on what will be the starting point of the natural time analysis. In the case of the 22 Pre-seismic SSTAs, there are 12 (55%) positive alarms that showed also critical points that there were observed from a few hours up to 28 days before the mainshock and 10 (~45%) for which there were SSTAs and Earthquake occurrence but no critical points. In the 16 false-positive SSTAs, there are 9 (~57%) cases where there were critical points (false-positive) and 7 (~43%) cases where there was only SSTAs and neither Earthquake nor NTA critical points. These last results, have the same percentages as in the previous case but they occurred in different SSTAs, hence, to not mistaken as similar.

In this analysis, the multi-parametric results showed, 69% positive alarms when putting together the results of the 8 PrePost and 12 Pre-Seismic SSTAs with the NTA and 31% false-positive that derives from the 9 NTA cases where there were critical points without the occurrence of Earthquakes.

All the results from the joint correlation analysis can be seen in Table 3.1 and 3.2 (for the '15 days before and same day from the first observation of SSTAs' Earthquake catalogs respectively) where the exact dates of seismic events, precursors (NTA critical points and TAs) as well as the magnitudes of each related Earthquake are reported. The difference between the dates of appearance of Earthquakes respect to the precursors and the distances between the barycenters and the epicenters of each case are also included in the table.

In conclusion, the analysis described in this chapter indicated that the joint correlation of RST and NTA on the Earthquake catalogs that started empirically 15 days prior to the first day of observation of SSTAs, provided better results than in the case where the catalogs analyzed in natural time started on the same day as the first day of observation of SSTAs.

The evolution of the Earthquake generation processes is complex and hard to define. Multi-parametric analysis can be applied in an attempt to better understand this complex system. In this study, the two parameters/methodologies (RST and NTA) that was implemented, did show some correlations with seismicity, yet, far more to be precise (epicenter and exact date) on the whereabouts of the mainshock. Further analyses has to be performed on the basis of these two methodologies in order to get a complete view on results and statistics. In example, the implementation of NTA on the seismicity that was already identified by RST on the 62 SSTAs could be done in addition to other parameters, which could be a change of the magnitude of completeness when acquiring the Earthquake catalogs and a multi buffer zone, meaning that the same analysis could be applied in various distances from the barycenters depending on the magnitude of the impending Earthquake and not only in a 150 km radius.

Table 3. 1 Joint correlation analysis. The 62 SSTAs are presented below in correlation with seismic events and natural time critical points ('15 days before' Earthquake catalogs). Orange color indicates the false-positive alarms of SSTAs, green color indicates the strong seismic events and red indicates the Post-Seismic SSTAs.

SSTAs	First TIR Observation	Date of related Earthquake	Magnitude	Date of NTA critical point	EQ-NTA	EQ-TIR	NTA-TIR	Distance from Barycenter (km)
1	11/7/2004	-	-	-	-	-	-	-
2	23/8/2004	24/8/2004	4,4	15/8/2004	9	1	-8	113
3	14/1/2005	31/1/2005	5,7	-	-	17	-	264
4	26/1/2005	12/1/2005	4	-	-	-14	-	121,6
5	27/2/2005	20/3/2005	4	20/2/2005	28	21	-7	102
6	21/3/2005	22/4/2005	4	12/3/2005	41	32	-9	111
7	4/5/2005	20/4/2005	4,1	-	-	-14	-	148
8	20/5/2005	-	-	-	-	-	-	-
9	13/12/2005	8/1/2006	6,4	-	-	26	-	221
10	16/12/2005	8/1/2006	6,4	24/12/2005	15	23	8	186
11	3/1/2006	8/1/2006	6,4	-	-	5	-	490
12	11/2/2006	21/2/2006	4,5	3/2/2006	18	10	-8	119
13	26/2/2006	21/2/2006	4,1	-	-	-5	-	142
14	18/3/2006	23/3/2006	4	20/3/2006	3	5	2	138
15	24/3/2006	13/4/2006	4,2	-	-	20	-	70
16	23/1/2007	-	-	19/1/2007	-	-	-4	-
17	24/1/2007	26/1/2007	4,2	-	-	2	-	139
18	18/2/2007	4/2/2007	4	-	-	-14	-	130
19	26/6/2007	6/7/2007	4,1	3/7/2007	3	10	7	53
20	27/6/2007	24/6/2007	4,3	23/6/2007	1	-3	-4	50
21	25/8/2007	28/8/2007	4,2	-	-	3	-	51
22	2/9/2007	29/9/2007	4	21/9/2007	8	27	19	53
23	2/9/2007	-	-	-	-	-	-	-
24	10/11/2007	-	-	9/11/2007	-	-	-1	-
25	11/1/2008	-	-	-	-	-	-	-
26	24/2/2008	-	-	12/3/2008	-	-	17	-
27	18/3/2008	19/3/2008	5	19/3/2008	0	1	1	132
28	12/4/2008	28/3/2008	5,1	-	-	-15	-	70
29	12/4/2008	-	-	25/4/2008	-	-	13	-
30	9/7/2008	15/7/2008	6,4	12/7/2008	3	6	3	536
31	3/12/2008	-	-	-	-	-	-	-
32	4/12/2008	13/12/2008	5,2	29/11/2008	14	9	-5	67
33	15/1/2009	16/1/2009	4,1	2/1/2009	14	1	-13	31
34	5/2/2009	-	-	15/2/2009	-	-	10	-
35	26/2/2009	16/3/2009	4,3	14/2/2009	30	18	-12	148
36	4/12/2009	-	-	19/11/2009	-	-	-15	-
37	1/1/2010	18/1/2010	5,2	8/1/2010	10	17	7	56
38	25/2/2010	9/3/2010	5,1	10/2/2010	27	12	-15	155,6
39	25/2/2010	12/3/2010	4,6	-	-	15	-	123
40	27/2/2010	26/3/2010	4,7	-	-	27	-	131
41	25/3/2010	4/4/2010	4,1	10/3/2010	25	10	-15	42
42	19/10/2010	23/10/2010	4,1	5/10/2010	18	4	-14	80,4
43	9/11/2010	-	-	30/10/2010	-	-	-10	-
44	9/11/2010	3/11/2010	5	-	-	-6	-	45,5
45	1/12/2010	-	-	-	-	-	-	-
46	13/12/2010	-	-	30/11/2010	-	-	-13	-
47	11/1/2011	10/2/2011	4,2	-	-	30	-	130
48	14/2/2011	11/2/2011	4,1	4/2/2011	7	-3	-10	125,7
49	6/12/2011	29/12/2011	4	-	-	23	-	147
50	13/12/2011	5/12/2011	4,1	-	-	-8	-	148
51	16/12/2011	29/12/2011	4	15/12/2011	14	13	-1	119,9
52	6/11/2012	3/12/2012	4,1	-	-	27	-	93,9
53	30/11/2012	3/12/2012	4,1	22/11/2012	11	3	-8	124,8
54	1/12/2012	-	-	-	-	-	-	-
55	19/1/2013	15/2/2013	4,6	27/1/2013	19	27	8	98,9
56	2/2/2013	30/1/2013	4	29/1/2013	1	-3	-4	86
57	2/2/2013	2/2/2013	4,1	26/1/2013	7	0	-7	100
58	3/2/2013	15/2/2013	4,6	-	-	12	-	24
59	16/2/2013	-	-	7/2/2013	-	-	-9	-
60	27/5/2013	15/6/2013	5,8	19/5/2013	27	19	-8	141
61	27/5/2013	6/6/2013	5	6/6/2013	0	10	10	52,9
62	2/10/2013	12/10/2013	6,2	20/9/2013	22	10	-12	261

Table 3. 2 Joint correlation analysis. The 62 SSTAs are presented below in correlation with seismic events and natural time critical points ('same day' Earthquake catalogs). Orange color indicates the false-positive alarms of SSTAs, green color indicates the strong seismic events and red indicates the Post-Seismic SSTAs.

SSTAs	First TIR Observation	Date of related Earthquake	Magnitude	Date of NTA critical point	EQ-NTA	EQ-TIR	NTA-TIR	Distance from Barycenter (km)
1	11/7/2004	-	-	-	-	-	-	-
2	23/8/2004	24/8/2004	4,4	-	-	1	-	113
3	14/1/2005	31/1/2005	5,7	29/1/2005	2	17	15	264
4	26/1/2005	12/1/2005	4	-	-	-	-	121,6
5	27/2/2005	20/3/2005	4	28/2/2005	20	21	1	102
6	21/3/2005	22/4/2005	4	23/3/2005	30	32	2	111
7	4/5/2005	20/4/2005	4,1	-	-	-	-	148
8	20/5/2005	-	-	-	-	-	-	-
9	13/12/2005	8/1/2006	6,4	-	-	26	-	221
10	16/12/2005	8/1/2006	6,4	-	-	23	-	186
11	3/1/2006	8/1/2006	6,4	-	-	5	-	490
12	11/2/2006	21/2/2006	4,5	19/2/2006	2	10	8	119
13	26/2/2006	21/2/2006	4,1	17/3/2006	-24	-	-	142
14	18/3/2006	23/3/2006	4	20/3/2006	3	5	2	138
15	24/3/2006	13/4/2006	4,2	-	-	20	-	70
16	23/1/2007	-	-	-	-	20	-	-
17	24/1/2007	26/1/2007	4,2	-	-	2	-	139
18	18/2/2007	4/2/2007	4	-	-	-14	-	130
19	26/6/2007	6/7/2007	4,1	30/6/2007	6	10	4	53
20	27/6/2007	24/6/2007	4,3	20/7/2007	-26	-4	23	50
21	25/8/2007	28/8/2007	4,2	-	-	3	-	51
22	2/9/2007	29/9/2007	4	-	-	27	-	53
23	2/9/2007	-	-	14/9/2007	-	-	12	-
24	10/11/2007	-	-	-	-	-	-	-
25	11/1/2008	-	-	-	-	-	-	-
26	24/2/2008	-	-	29/3/2008	-	-	34	-
27	18/3/2008	19/3/2008	5	-	-	1	-	132
28	12/4/2008	28/3/2008	5,1	19/4/2008	-22	-15	7	70
29	12/4/2008	-	-	16/4/2008	-	-	4	-
30	9/7/2008	15/7/2008	6,4	-	-	6	-	536
31	3/12/2008	-	-	31/12/2008	-	-	28	-
32	4/12/2008	13/12/2008	5,2	12/12/2008	1	9	8	67
33	15/1/2009	16/1/2009	4,1	-	-	1	-	31
34	5/2/2009	-	-	-	-	-	-	-
35	26/2/2009	16/3/2009	4,3	27/2/2009	17	18	1	148
36	4/12/2009	-	-	5/12/2009	-	-	1	-
37	1/1/2010	18/1/2010	5,2	-	-	17	-	56
38	25/2/2010	9/3/2010	5,1	25/2/2010	12	12	0	155,6
39	25/2/2010	12/3/2010	4,6	5/3/2010	7	15	8	123
40	27/2/2010	26/3/2010	4,7	11/3/2010	15	27	12	131
41	25/3/2010	4/4/2010	4,1	25/3/2010	10	10	0	42
42	19/10/2010	23/10/2010	4,1	20/10/2010	3	4	1	80,4
43	9/11/2010	-	-	11/11/2010	-	-	2	-
44	9/11/2010	3/11/2010	5	-	-	-6	-	45,5
45	1/12/2010	-	-	1/12/2010	-	-	0	-
46	13/12/2010	-	-	15/12/2010	-	-	2	-
47	11/1/2011	10/2/2011	4,2	13/1/2011	28	30	2	130
48	14/2/2011	11/2/2011	4,1	19/2/2011	-8	-3	5	125,7
49	6/12/2011	29/12/2011	4	14/12/2011	15	23	8	147
50	13/12/2011	5/12/2011	4,1	-	-	-8	-	148
51	16/12/2011	29/12/2011	4	19/12/2011	10	13	3	119,9
52	6/11/2012	3/12/2012	4,1	29/11/2012	4	27	23	93,9
53	30/11/2012	3/12/2012	4,1	-	-	3	-	124,8
54	1/12/2012	-	-	-	-	-	-	-
55	19/1/2013	15/2/2013	4,6	-	-	27	-	98,9
56	2/2/2013	30/1/2013	4	-	-	-3	-	86
57	2/2/2013	2/2/2013	4,1	-	-	0	-	100
58	3/2/2013	15/2/2013	4,6	15/2/2013	0	12	12	24
59	16/2/2013	-	-	22/2/2013	-	-	6	-
60	27/5/2013	15/6/2013	5,8	-	-	19	-	141
61	27/5/2013	6/6/2013	5	31/5/2013	6	10	4	52,9
62	2/10/2013	12/10/2013	6,2	-	-	10	-	261

Conclusions

In the present work, a barycentral approach have been applied on the previously 62 SSTAs that were identified by RST approach. In particular, it was applied in order to reduce the area that was suggested formerly for the impending seismicity and provide a more precise alarm zone, always in respect to the pre-defined space-time rules. Thus, to receive an indication on the reliability of this approach which is measured by the fraction of SSTAs occurred in the investigated area/period preceded or followed by Earthquakes with $M \geq 4$ in the prescribed space-time correlation window as potential indicator of occurred or impending seismic activity. In particular:

- 15 (~24%) SSTAs occurred before and after the seismic events (PRE-POST seismic SSTAs);
- 22 (~35%) SSTAs occurred only before the seismic events (PRE seismic SSTAs);
- 9 (~15%) SSTAs occurred only after the seismic events (POST seismic SSTAs);
- 16 (~26%) false-positive SSTAs (observed thermal anomalies with absence of seismicity ($M \geq 4$) in the time-space window).

The barycentral analysis showed 74% of the 62 SSTAs in apparent space-time relation with earthquake occurrence and 26% false-positive alarms. The barycentral approach showed also a disadvantage. It can 'miss' some Earthquake events that might be related to the SSTAs. This happens due to the distance reduction between the epicenters (depending on the magnitude) and the barycenters that represents the whole/merged STAs. To avoid this kind of problem, as a future study, one could implement an analysis in a moving barycenter, not on the merged STAs but following each day the TAs barycenter and then create alarm zones.

In this study, the natural time analysis has been carried out in order to understand if and when there is an indication of a critical point. In particular, it was used to better understand when the system enters a critical stage, in example, before or after the 62 SSTAs and how many days before the mainshocks, which were related to the appearance of the SSTAs. The analysis was done in two scales. Firstly, on Earthquake catalogs that had a starting date, 15 days before the first day of SSTAs observation and secondly on Earthquake catalogs that had a starting date, the same day as the first day of SSTAs observation. The choices of the starting points of the Earthquake catalogs

were made empirically. Notably, in such an analysis, is better to choose a bigger time series of Earthquakes, taking into account the seismicity in a period prior to the appearance of SSTAs, in order to have a better understanding on the preparation phase of the impending Earthquake as the results showed. The choice of the starting point of the natural time analysis is a challenge and yet it might need more parameters to better define it.

The multi-parametric results, regarding the ‘NTA, 15 days before the first day of SSTAs observation’ showed 73% positive alarms and the ‘NTA, same day as the first day of SSTAs observation’ showed 69% positive alarms, for a possible seismic hazard forecast.

An advantage using a multi-parametric analysis, even if, on the RST analysis, there are days where the presence of clouds in the scene does not allow the continuous monitoring of the thermal anomalies, using a second parameter (in this case, NTA) to track the evolution of seismicity, can provide information on the preparation phase of a strong event. Finally, in order to be more precise in some kind of Earthquake predictions, the combined use with other parameters based on observations of different nature (i.e. seismological, geochemical, geodetic, etc.) and create an integrated system with multi-parametric analysis could improve seismic hazard assessment in the short-term.

References

Aliano C, Corrado R, Filizzola C, Genzano N, Pergola N, Tramutoli V (2007a) From GMOSS to GMES: Robust TIR Satellite Techniques for Earthquake active regions monitoring. Glob Monit Secur Stab - Integr Sci Technol Res Support Secur Asp Eur Union, EU-report EUR 23033 EN 320–330. doi:10.2788/53480.

Aliano C, Corrado R, Filizzola C, Pergola N, Tramutoli V (2007b) Robust Satellite Techniques (RST) for Seismically Active Areas Monitoring: the Case of 21st May, 2003 Boumerdes/Thenia (Algeria) Earthquake. 2007 Int. Work. Anal. Multi-temporal Remote Sens. Images. IEEE, pp 1–6.

Aliano C, Corrado R, Filizzola C, Genzano N, Pergola N, Tramutoli V (2008a) Robust TIR satellite techniques for monitoring earthquake active regions: limits, main achievements and perspectives. Ann Geophys 51:303–317.

Aliano C, Corrado R, Filizzola C, Pergola N, Tramutoli V (2008b) Robust satellite techniques (RST) for the thermal monitoring of earthquake prone areas: the case of Umbria-Marche October, 1997 seismic events. Ann Geophys 51:451–459.

Aliano C, Martinelli G, Filizzola C, Pergola N, Genzano N, Tramutoli V (2008c) Robust Satellite Techniques for monitoring TIR anomalies in seismogenic areas. 2008 Second Work. Use Remote Sens. Tech. Monit. Volcanoes Seism. Areas. IEEE, pp 1–7.

Aliano C, Corrado R, Filizzola C, Genzano N, Lanorte V, Mazzeo G, Pergola N, Tramutoli V (2009) Robust Satellite Techniques (RST) for monitoring thermal anomalies in seismically active areas. 2009 IEEE Int. Geosci. Remote Sens. Symp. IEEE, pp III–65–III–68.

Bonfanti P, Genzano N, Heinicke J, Italiano F, Martinelli G, Pergola N, Telesca L, Tramutoli V (2012) Evidence of CO₂- gas emission variations in the central Apennines (Italy) during the L'Aquila seismic sequence (March-April 2009). Boll Di Geofis Teor ed Appl 53:147–168. doi:10.4430/bgta0043.

Corrado R., Caputo R., Filizzola C., Pergola N., Pietrapertosa C. and Tramutoli V.: Seismically active area monitoring by robust TIR satellite techniques: a sensitivity analysis on low magnitude Earthquakes in Greece and Turkey. *Natural Hazards and Earth System Sciences* (2005) 5: 101-108.

Cuomo, V., Filizzola, C., Pergola, N., Pietrapertosa, C. and Tramutoli, V.: A self-sufficient approach for GERB cloudy radiance detection, *Atmos. Res.*, 72, 39–56, 2004.

Di Bello G, Filizzola C, Lacava T, Marchese F, Pergola N, Pietrapertosa C, Piscitelli S, Scaffidi I, Tramutoli V (2004) Robust Satellite Techniques for Volcanic and Seismic Hazards Monitoring. *Ann Geophys* 47:49–64.

Dobrovolsky, I. P., Zubkov, S. I. and Miachkin, V. I.: Estimation of the size of Earthquake preparation zones, *Pure Appl. Geophys. PAGEOPH*, 117, 1025–1044, doi: 10.1007/BF00876083, 1979.

Eleftheriou, C. Filizzola, N. Genzano, T. Lacava, M. Lisi, R. Paciello, N. Pergola, F. Vallianatos, V. Tramutoli, “Long-Term RST Analysis of Anomalous TIR Sequences in Relation with Earthquakes Occurred in Greece in the Period 2004–2013”. In *Pure and Applied Geophysics*, vol. 173 (2016), pp. 285-303. Doi: 10.1007/s00024-015-1116-8.

Eneva M, Adams D, Wechsler N, Ben-zion Y, dor o (2008) Thermal properties of faults in southern California from remote sensing data. 71.

Filizzola, C., Pergola, N., Pietrapertosa, C. and Tramutoli, V.: Robust satellite techniques for seismically active areas monitoring: a sensitivity analysis on September 7, 1999 Athens’s Earthquake, *Phys. Chem. Earth*, 29(4-9), 517–527, doi:10.1016/j.pce.2003.11.019, 2004.

Genzano, N., Aliano, C., Filizzola, C., Pergola, N. and Tramutoli, V.: Robust satellite technique for monitoring seismically active areas: The case of Bhuj-Gujarat Earthquake, *Tectonophysics*, 431, 197–210, 2007.

Genzano, N., Aliano, C., Corrado, R., Filizzola, C., Lisi, M., Mazzeo, G., Paciello, R., Pergola, N. and Tramutoli, V.: RST analysis of MSG-SEVIRI TIR radiances at the time of the Abruzzo 6 April 2009 Earthquake, *Nat. Hazards Earth Syst. Sci.*, 9, 2073–2084, 2009a.

Genzano, N., Aliano, C., Corrado, R., Filizzola, C., Lisi, M., Paciello, R., Pergola, N., Tsamalashvili, T. and Tramutoli, V.: Assessing of the robust satellite techniques (RST) in areas with moderate seismicity, in *Proceedings of Multitemp 2009*, pp. 307–314, Mystic, Connecticut, USA, 28-30 July 2009., 2009b.

Genzano N, Corrado R, Coviello I, Grimaldi Csl, Filizzola C, Lacava T, Lisi M, Marchese F, Mazzeo G, Paciello R, Pergola N, Tramutoli V (2010) A multi-sensors analysis of RST-based thermal anomalies in the case of the Abruzzo earthquake. 2010 IEEE Int. Geosci. Remote Sens. Symp. IEEE, pp 761–764.

Genzano N. (2014): Robust Satellite Techniques (RST) for seismically active area monitoring: improvements and long term validation on nine years (2004-2012) of MSG-SEVIRI TIR observations over Italy (PhD, thesis).

Genzano N, Filizzola C, Paciello R, Pergola N, Tramutoli V (2015) Robust Satellite Techniques (RST) for monitoring Earthquake prone areas by satellite TIR observations: the case of 1999 Chi-Chi earthquake (Taiwan). *J Asian Earth Sci.* doi:10.1016/j.jseaes.2015.02.010.

Lazaridou-Varotsos, Mary S.: Earthquake Prediction by Seismic Electric Signals, The success of the VAN method over thirty years, 2013, XVIII, 254 p., ISBN 978-3-642-24406-3.

Lisi M, Filizzola C, Genzano N, Grimaldi Csl, Lacava T, Marchese F, Mazzeo G, Pergola N, Tramutoli V (2010) A study on the Abruzzo 6 April 2009 earthquake by applying the RST approach to 15 years of AVHRR TIR observations. *Nat Hazards Earth Syst Sci* 10:395–406. doi:10.5194/nhess-10-395-2010.

Pergola N, Aliano C, Coviello I, Filizzola C, Genzano N, Lacava T, Lisi M, Mazzeo G, Tramutoli V (2010) Using RST approach and EOS-MODIS radiances for monitoring seismically active regions: a study on the 6 April 2009 Abruzzo earthquake. *Nat Hazards Earth Syst Sci* 10:239–249. doi:10.5194/nhess-10-239-2010.

Pietrapertosa, C., Pergola, N., Lanorte, V. and Tramutoli, V.: Self adaptive algorithms for change detection: OCA (the one-channel cloud-detection approach) an adjustable method for cloudy and clear radiances detection, in *Technical Proceedings of the Eleventh International (A)TOVS Study Conference (ITSC-XI) Budapest, Hungary, 20-26 September 2000*, Bureau of Meteorology Research Centre, edited by J. D. (Eds. . Le Marshall, J.F., Jasper, pp. 281–291, Melbourne, Australia., 2001.

Pulinets Sa, Biagi P, Tramutoli V, Legen'ka Ad, Depuev Vk (2007) Irpinia Earthquake 23 November 1980 - Lesson from Nature reviled by joint data an analysis. *Ann Geophys* 50:61–78.

Sarlis, N.V., Skordas, E.S., Lazaridou, M.S., Varotsos, P.A., 2008. Investigation of seismicity after the initiation of a seismic electric signal activity until the main shock. *Proc. Jpn. Acad. Ser. B* 84, 331–343.

Scholz Ch, Sykes Lr, Aggarwal Yp (1973) Earthquake prediction: a physical basis. *Science* 181(4102):803–810. doi:10.1126/science.181.4102.803.

Tramutoli, V.: Robust AVHRR Techniques (RAT) for Environmental Monitoring: theory and applications, in *Proceedings of SPIE*, vol. 3496, edited by E. Zilioli, pp. 101–113., 1998.

Tramutoli V, Lanorte V, Pergola N, Pietrapertosa C, Ricciardelli E, Romano F (2000). Self-adaptive algorithms for environmental monitoring by SEVIRI and GERB: a preliminary study. *Proc. EUMETSAT Meteorol. Satell. data User's Conf. Bol. Italy*, 29 May - 2 June, 2000. Bologna, Italy, pp 79–87.

Tramutoli V., Di Bello G., Pergola N. and Piscitelli S.: Robust satellite techniques for remote sensing of seismically active areas, *Ann. di Geofis.*, 44(2), 295–312, 2001.

Tramutoli V., Cuomo V., Filizzola C., Pergola N. and Pietrapertosa C.: Assessing the potential of thermal infrared satellite surveys for monitoring seismically active areas: The case of Kocaeli (İzmit) Earthquake, August 17, 1999, *Remote Sens. Environ.*, 96(3-4), 409–426, doi:10.1016/j.rse.2005.04.006, 2005.

Tramutoli V (2007) Robust Satellite Techniques (RST) for Natural and Environmental Hazards Monitoring and Mitigation: Theory and Applications. 2007 Int. Work. Anal. Multi-temporal Remote Sens. Images. IEEE, pp 1–6.

Tramutoli V, Aliano C, Corrado R, Filizzola C, Genzano N, Lisi M, Lanorte V, Tsamalashvili T (2009) Abrupt change in greenhouse gases emission rate as a possible genetic model of TIR anomalies observed from satellite in Earthquake active regions. *Proc. ISRSE 2009*. pp 567–570.

Tramutoli V, Inan S, Jakowski N, Pulinets S, Romanov A, Filizzola C, Shagimuratov I, Pergola N, Ouzounov D, Papadopoulos G, Genzano N, Lisi M, Corrado R, Alparslan E, Wilken V, Tsybulia K, Romanov A, Paciello R, Coviello I, Zakharenkova I, Romano G, Cherniak Y (2012a) The PREEARTHQUAKES EU-Fp7 Project: Preliminary Results of the PRIME Experiment for a Dynamic Assessment of Seismic Risk (DASR) by Multiparametric Observations. 31_ Convegno Naz. Grup. Naz. di Geofis. della Terra Solida (GNGTS). 20-22 novembre, Potenza. Potenza, pp 384–388.

Tramutoli V, Inan S, Jakowski N, Pulinets Sa, Romanov A, Filizzola C, Shagimuratov I, Pergola N, Genzano N, Serio C, Lisi M, Corrado R, Grimaldi Csl, Faruolo M, Petracca R, Ergintav E, C, Akir Z, Alparslan E, Gurol S, Mainul Hoque M, Missling Kd, Wilken V, Borries C, Kalilnin Y, Tsybulia K, Ginzburg E, Pokhunkov A, Pustivalova L, Romanov A, Cherny I, Trusov S, Adjalova A, Ermolaev D, Bobrovsky S, Paciello R, Coviello I, Falconieri A, Zakharenkova I, Cherniak Y, Radievsky A, Lapenna V, Balasco M, Piscitelli S, Lacava T, Mazzeo

G (2012b) PRE-EARTHQUAKES, an Fp7 Project for Integrating Observations and Knowledge on Earthquake Precursors: Preliminary Results and Strategy. 2012 IEEE Int. Geosci. Remote Sens. Symp. IEEE, Munich, pp 3536–3539.

Tramutoli V., Aliano C., Corrado R., Filizzola C., Genzano N., Lisi M., Martinelli G. And Pergola N.: On the possible origin of thermal infrared radiation (TIR) anomalies in Earthquake prone areas observed using robust satellite techniques (RST), *Chem. Geol.*, 339, 157–168, doi:10.1016/j.chemgeo.2012.10.042, 2013.

Tramutoli V, Corrado R, Filizzola C, Genzano N, Lisi M, Paciello R, Pergola N, Sileo G (2013b) A decade of RST applications to seismically active areas monitoring by TIR satellite observations. 2013 EUMETSAT Meteorol. Satell. Conf. & 19th Am. Meteorol. Soc. Satell. Meteorol. Oceanogr. Climatol. Conf. p 8 pp.

Tramutoli V, Corrado R, Filizzola C, Genzano N, Lisi M, Paciello R, Pergola N (2015b) One year of RST based satellite thermal monitoring over two Italian seismic areas. *Boll Di Geofis Teor ed Appl.* doi:10.4430/bgta0150.

Vallianatos, F., Michas, G., Hloupis, G. (2015) Multiresolution wavelets and natural time analysis before the January-February 2014 Cephalonia (Mw6.1 & 6.0) sequence of strong earthquake events. *Physics and Chemistry of the Earth* 85-86, pp. 201-209.

Varotsos P., K. Alexopoulos and K. Nomicos, Seismic electric currents, *Practica Athens Academy* 56, 277–286, 1981.

Varotsos P., K. Alexopoulos, K. Nomicos and M. Lazaridou, Earthquake prediction and electric signals, *Nature* 322, 120, 1986.

Varotsos P., N. Sarlis, and E. Skordas, Spatiotemporal complexity aspects on the interrelation between Seismic Electric Signals and seismicity, *Practica of Athens Academy*, 76, 294–321, 2001.

Varotsos P. A., N.V. Sarlis, E.S. Skordas, S. Uyeda and M. Kamogawa, Natural time analysis of critical phenomena: The case of seismicity, EPL 92, 29002, 2010.

Varotsos P., N. Sarlis, E. Skordas, S. Uyeda and M. Komogawa, Natural time analysis of critical phenomena, Proc. Natl. Acad. Sci. USA, 108, 11361–11364, 2011.

Varotsos Panayiotis A., Nicholas V. Sarlis, Efthimios S. Skordas. Identifying the occurrence time of an impending mainshock: a very recent case. Earthq Sci (2015) 28(3):215–222, DOI 10.1007/s11589-015-0122-3.

Web sites

<http://www.gein.noa.gr/en/> - 2016

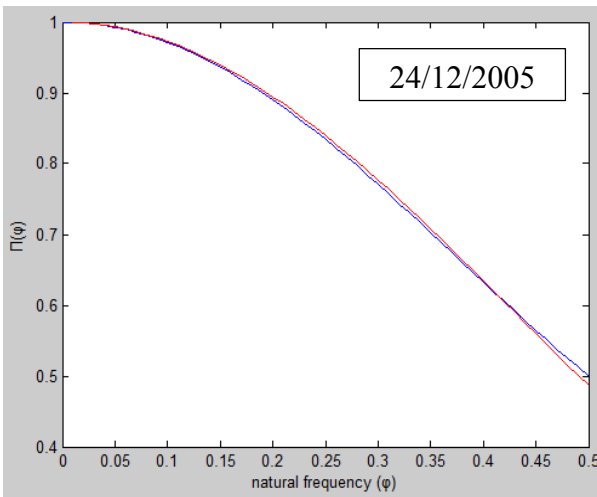
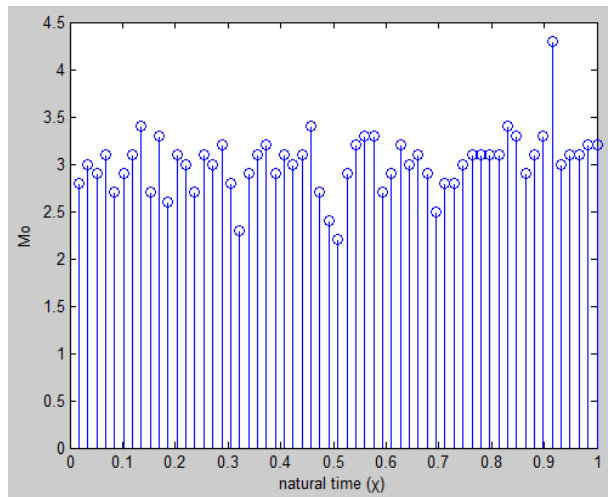
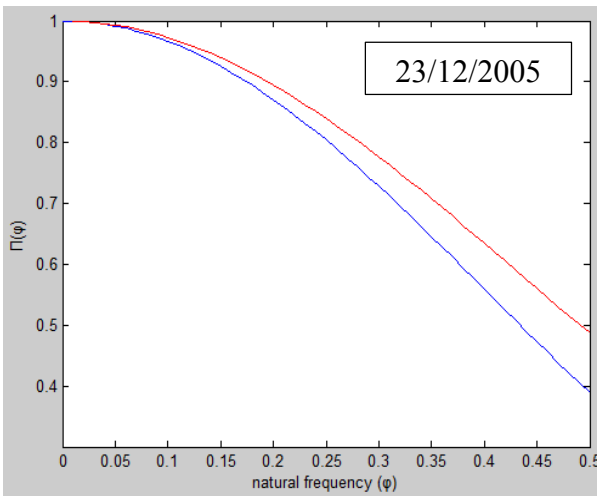
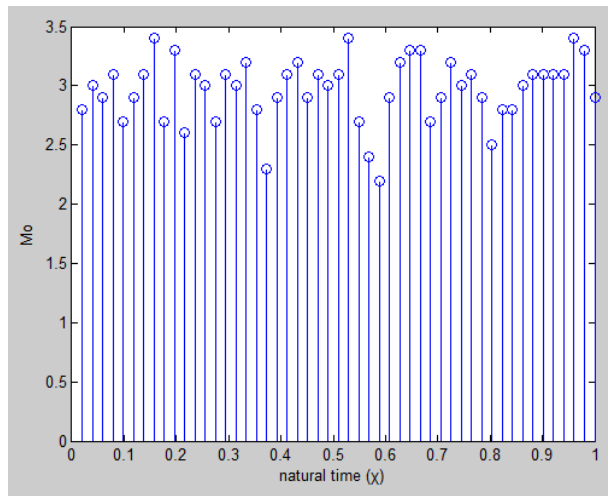
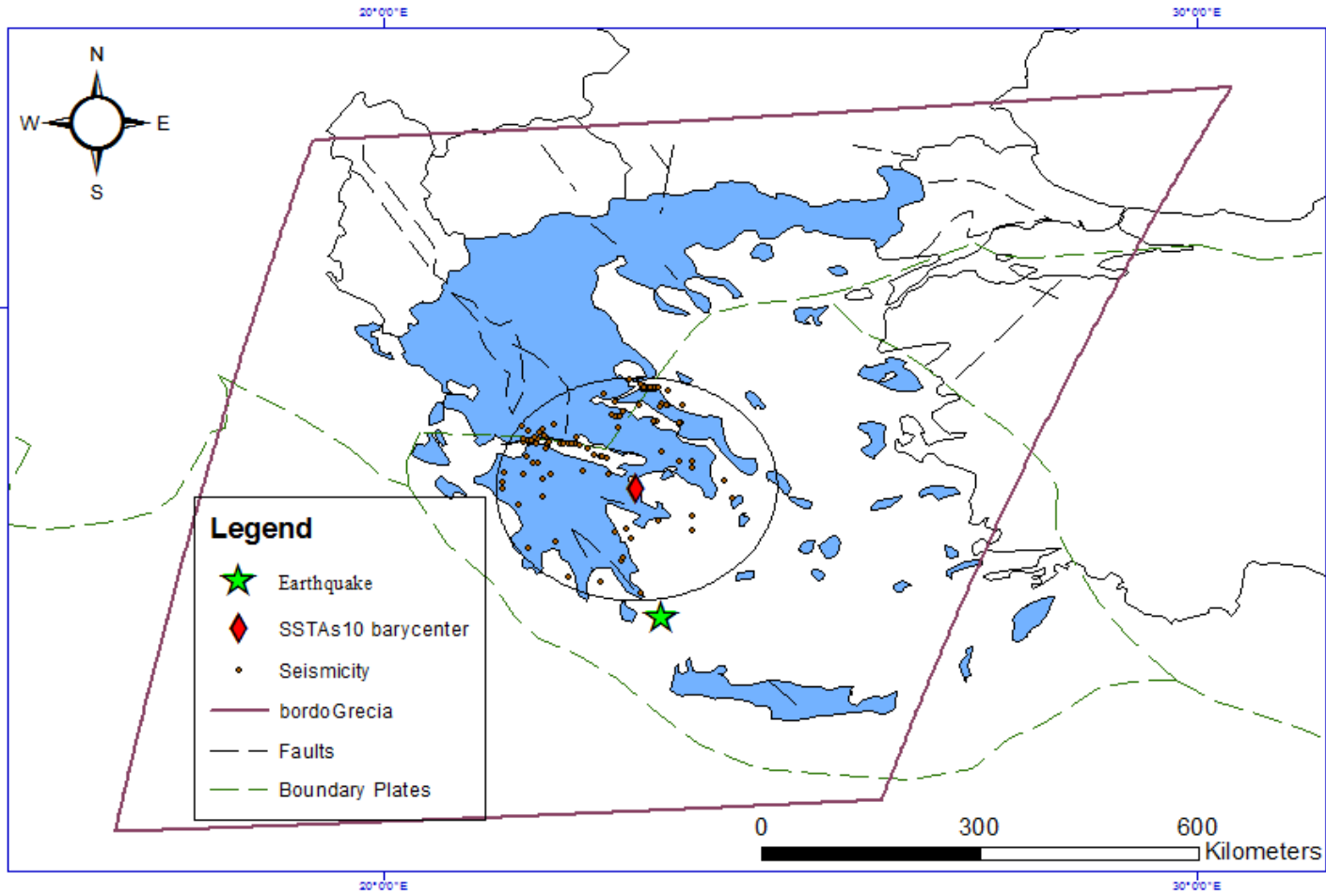
<http://www.esri.com/> - 2016

<http://gredass.unife.it/> - 2016

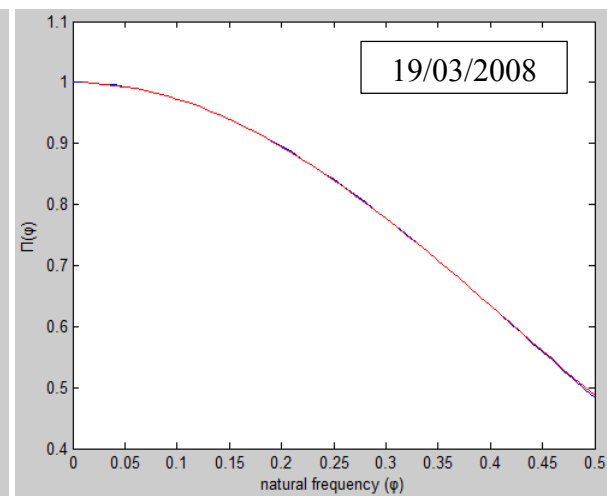
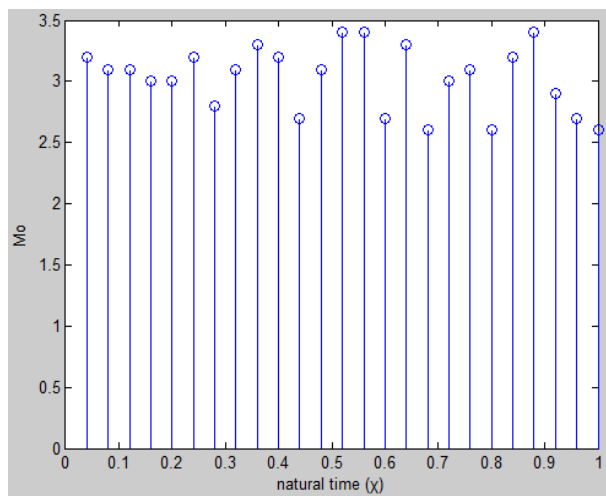
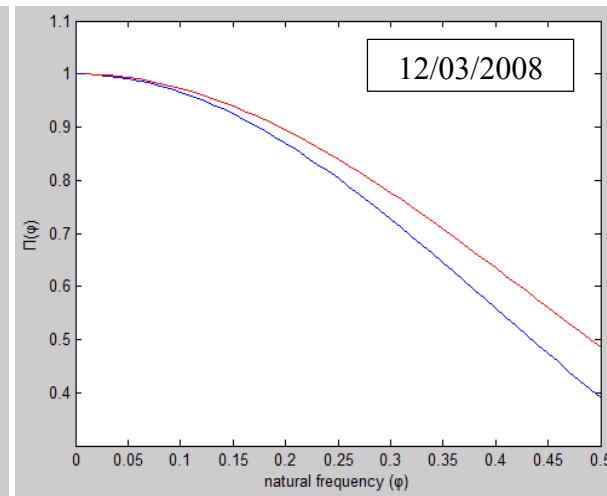
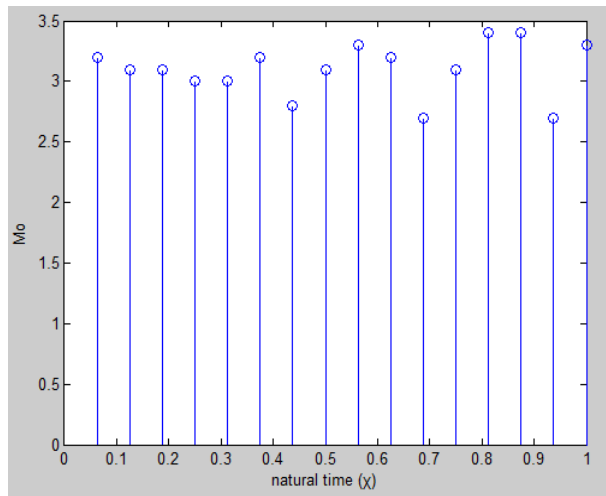
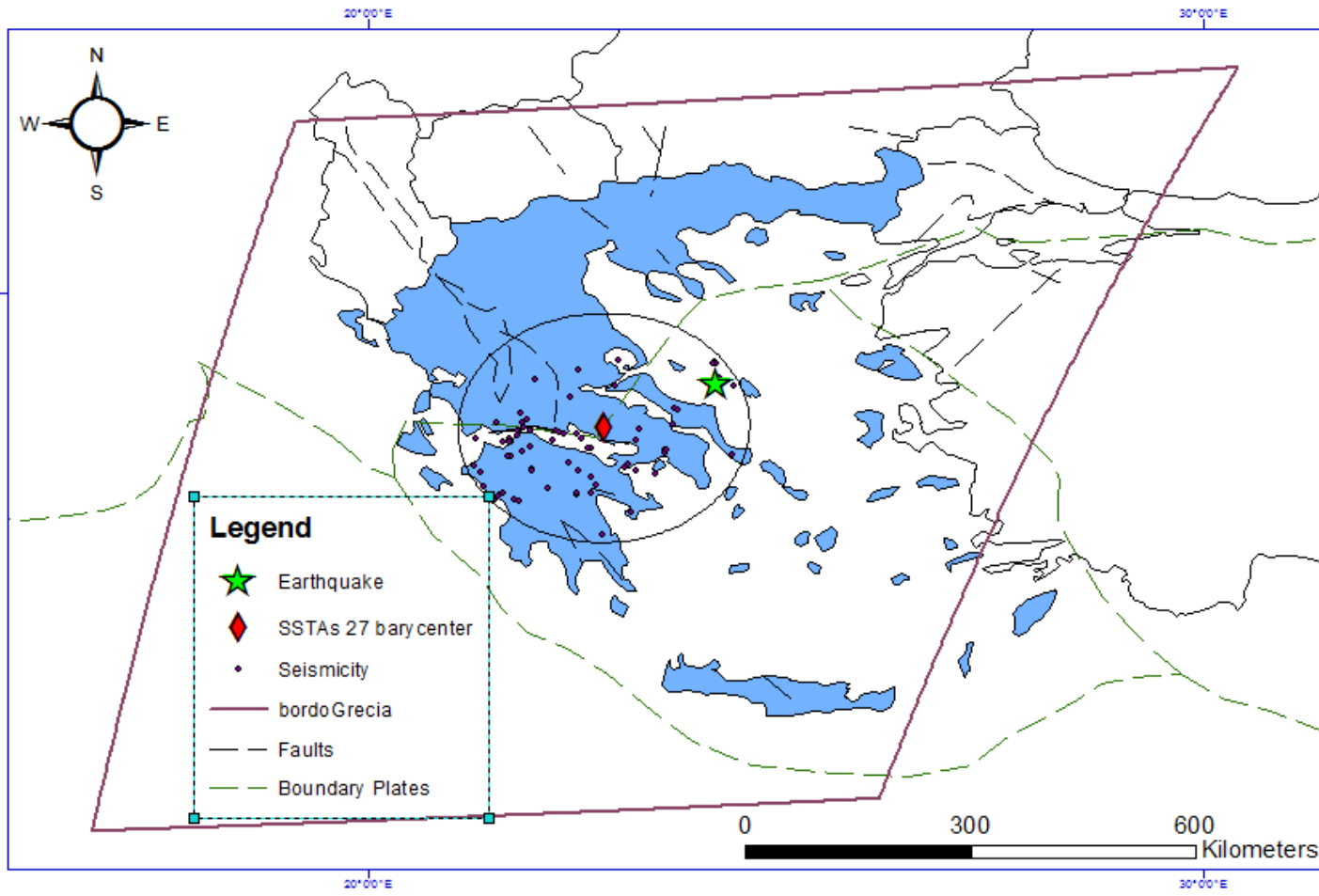
Annex – Natural time analysis for strong Earthquake events

The natural time analysis was performed on Earthquake catalogs starting 15 days before and same day as the first day of TIR anomalies observations. Here are presented the results of the NTA that was done on Earthquake catalogs starting 15 days before the first day of TIR anomalies observations (for those considered PRE-seismic SSTAs) for seismic events with magnitude $M \geq 5$. The ID number of SSTAs that are presented below in correlation with the critical points that the NTA showed, can be seen in more detail in figure 2.6 above. The maps shows the barycenter of each sequence, the seismicity that was analyzed in a 150km buffer zone as well as the mainshock. On the left images are the seismic events in natural time domain. On the right images are plotted the relative power spectrum $\Pi(\varphi)$ according to the natural frequency φ . In red is plotted the theoretical curve described in Varotsos et al. (2001).

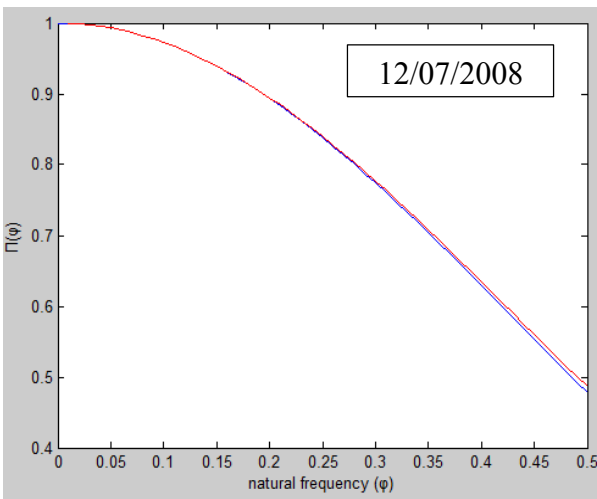
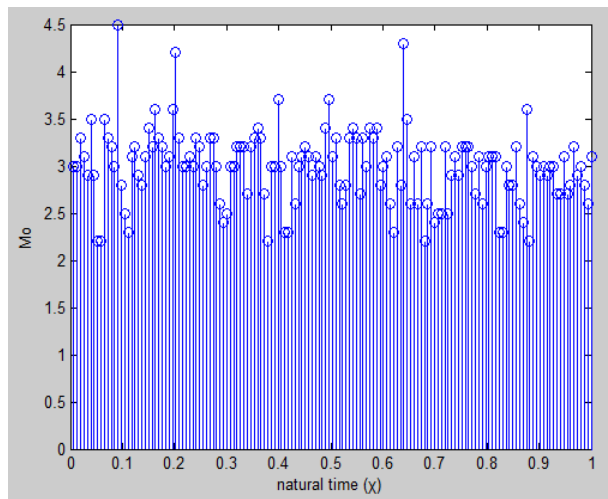
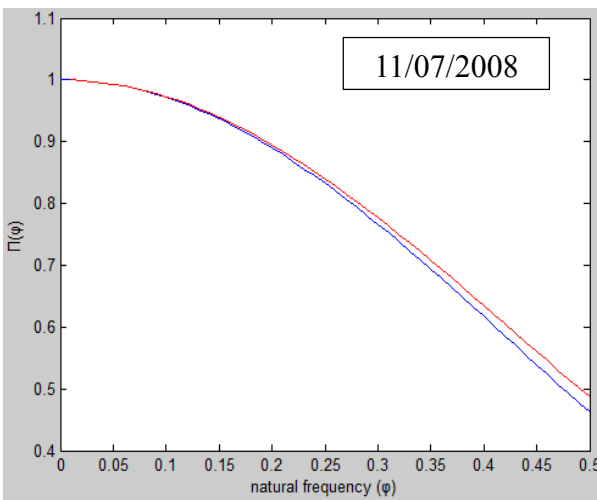
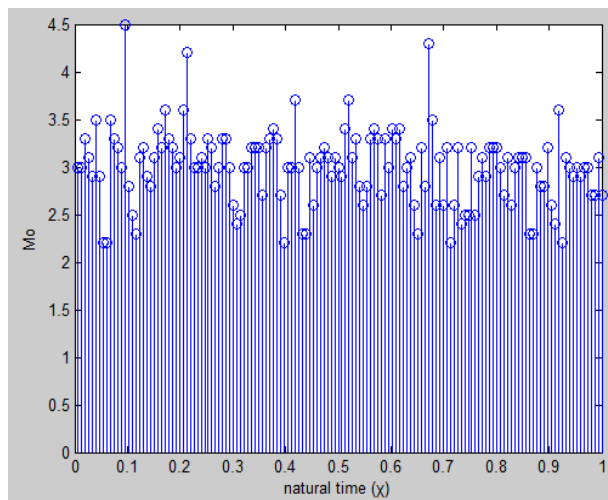
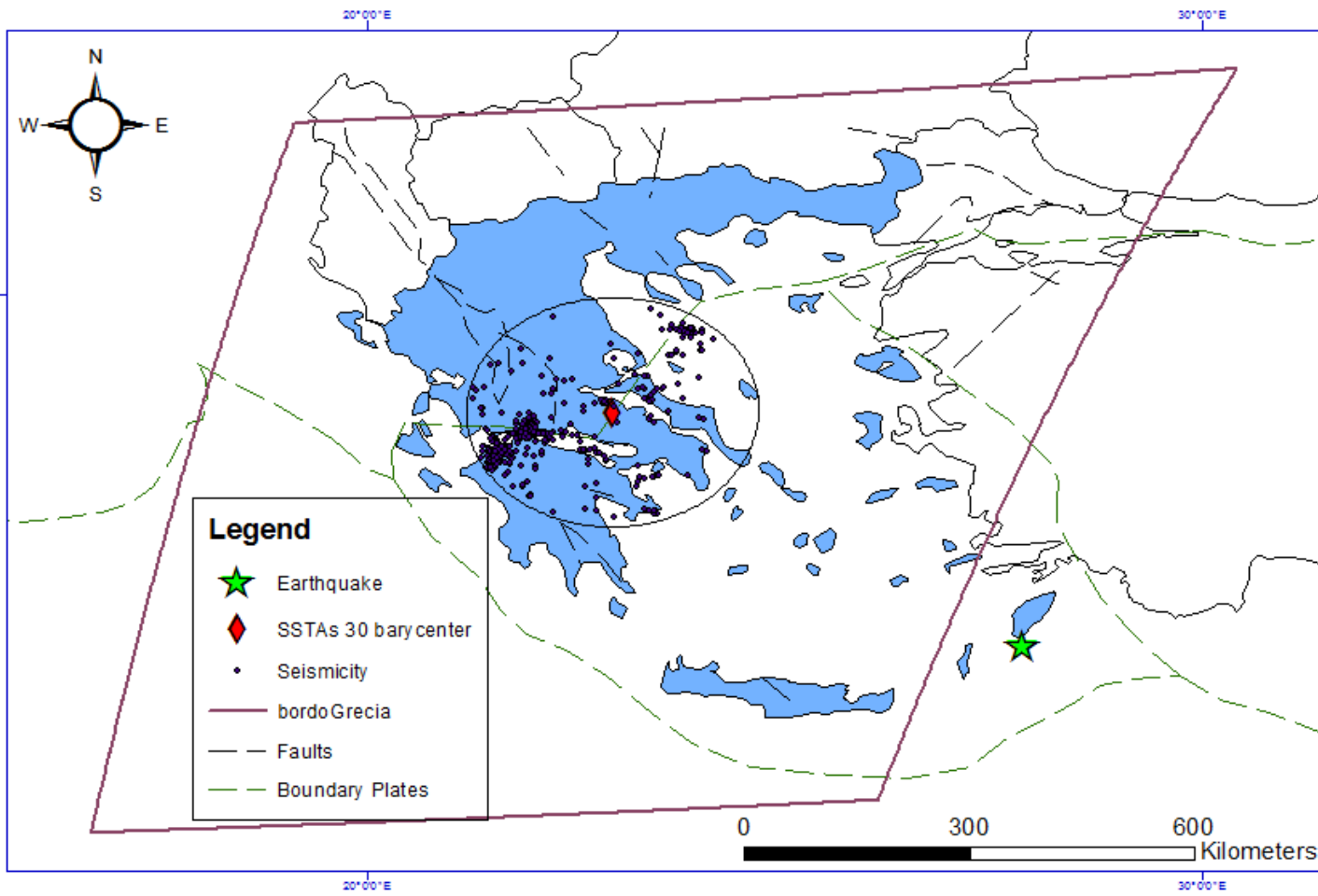
SSTAs 10 (Ionian-Peloponnese-Central) on 16-18/12/2005 Earthquake on 8/1/2006 (M=6.4)



SSTAs 27 (Ionian-Peloponnese-Central) on 18-19/3/2008 Earthquake on 19/03/2008 M=5.0

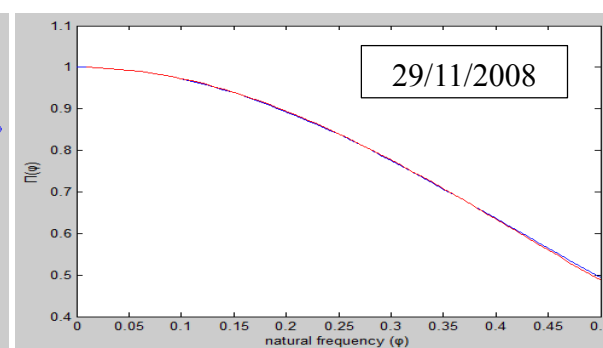
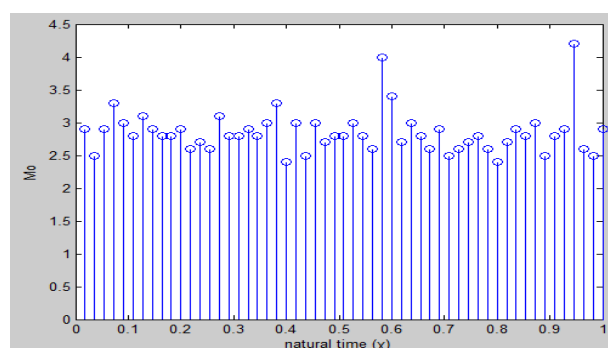
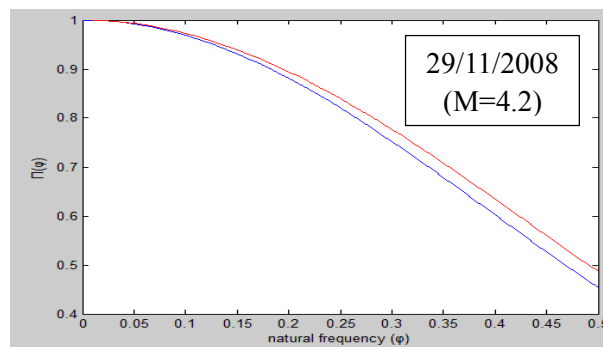
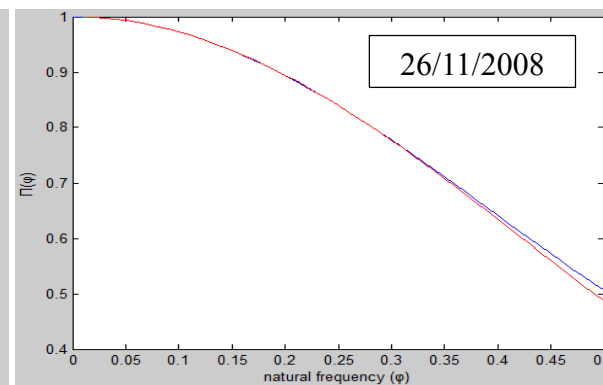
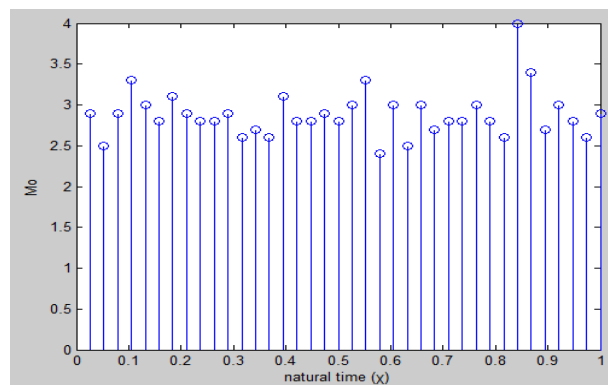
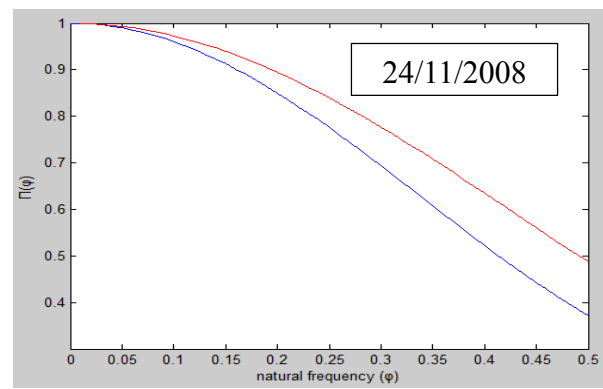
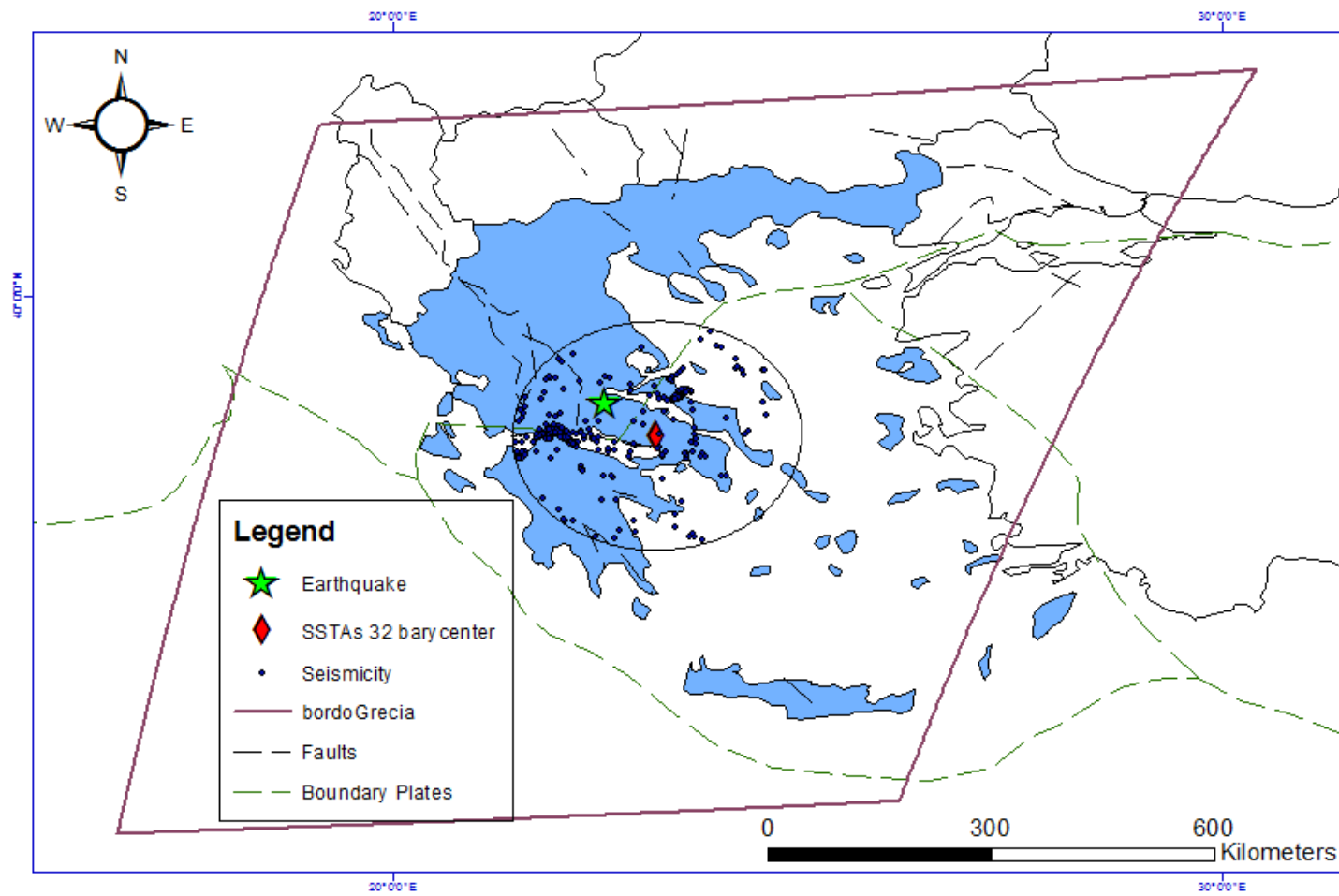


SSTAs 30 (Ionian-Peloponnese-Central) on 9,16,23/7/2008 Earthquake on 15/7/2008 M=6,4

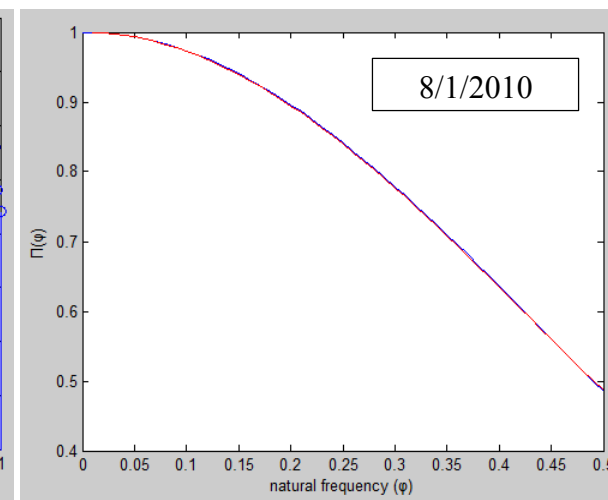
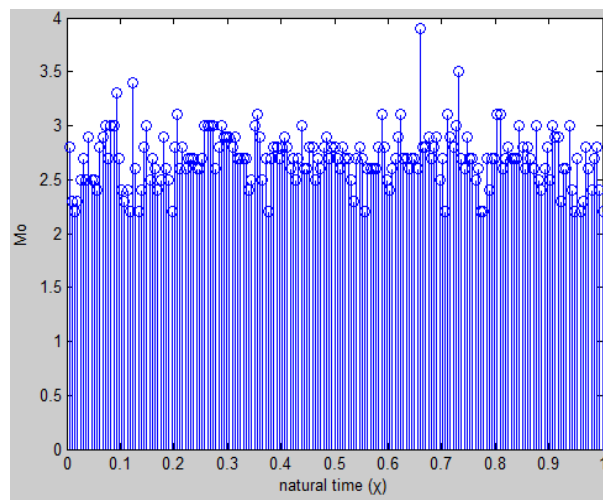
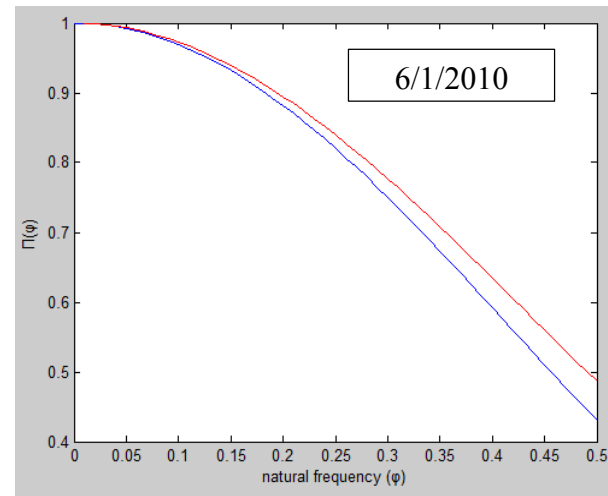
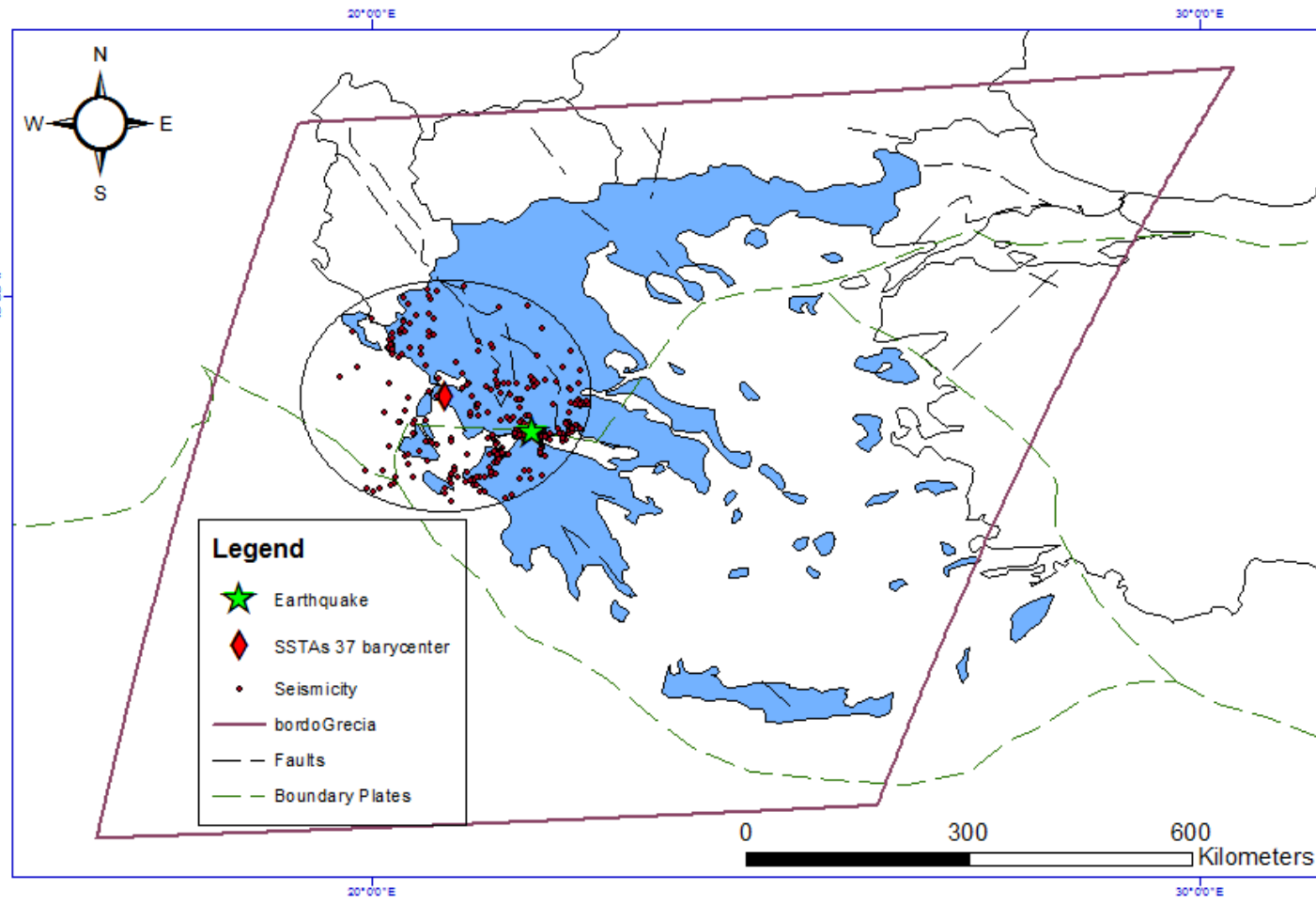


SSTAs 32 (Ionian-Peloponnese-Central) on 4,5,7/12/2008 **Earthquake** on 13/12/2008 M=5.2

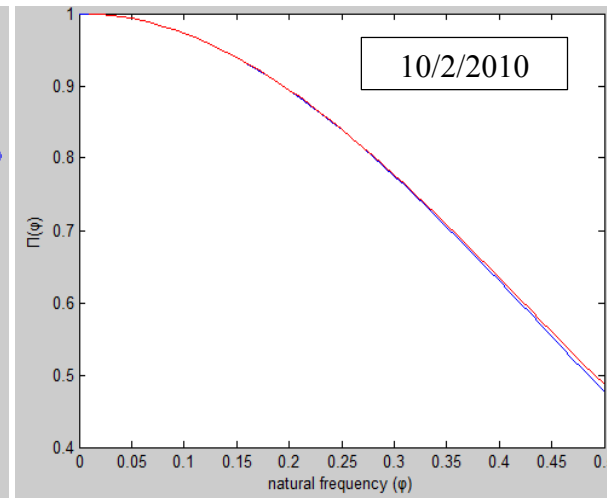
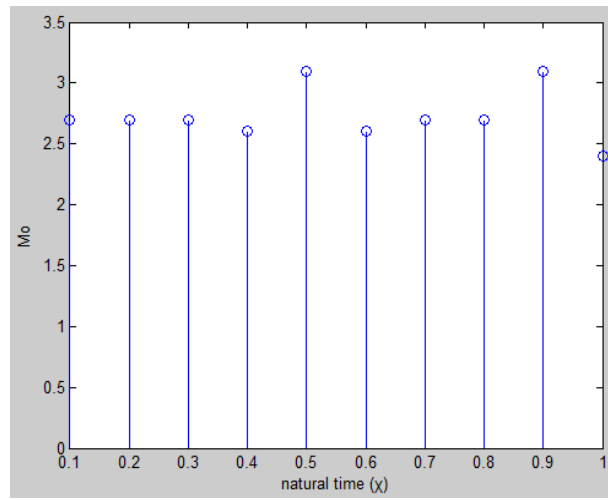
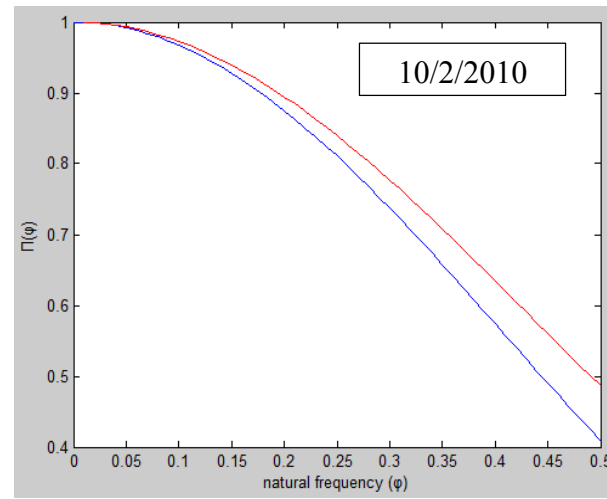
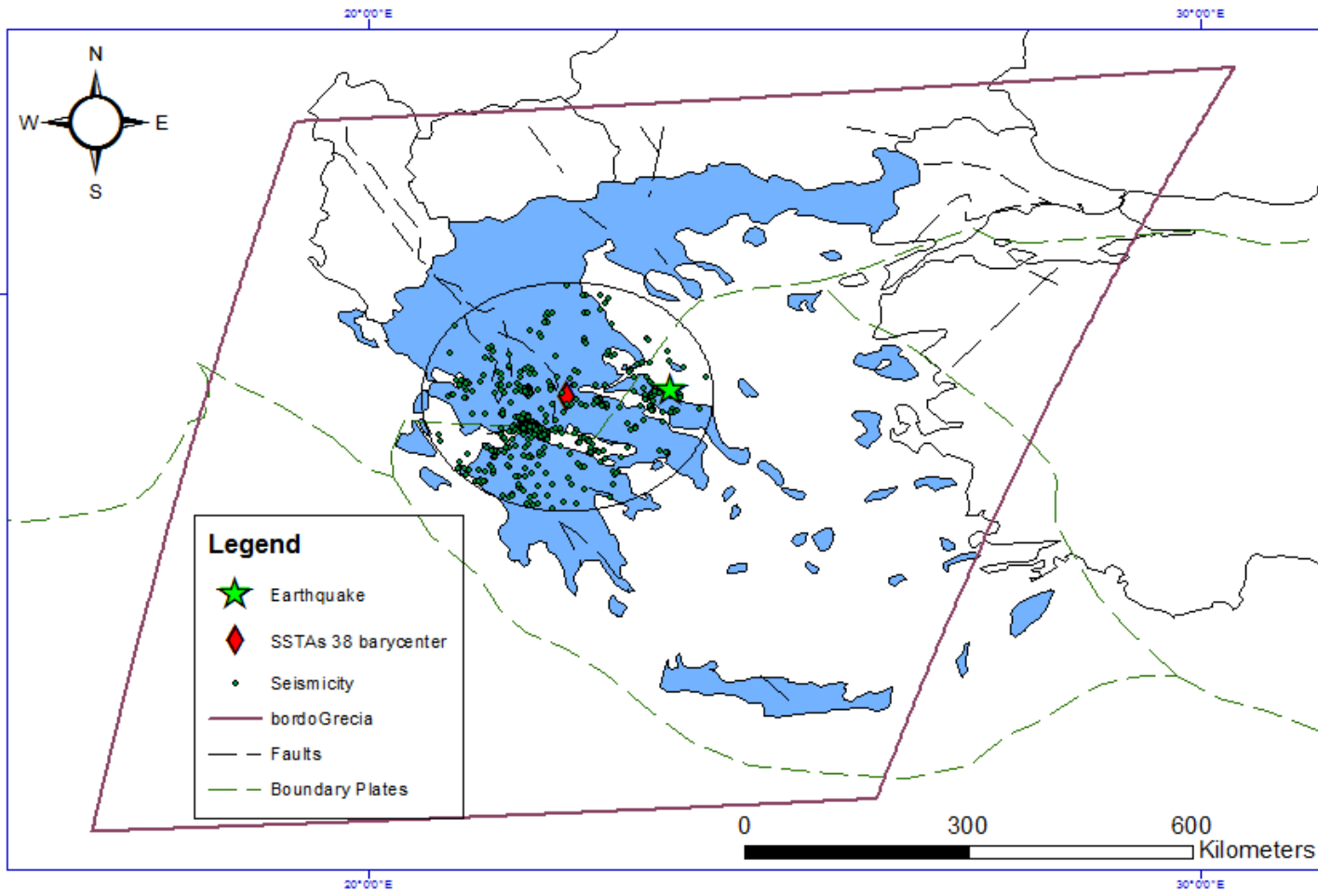
(NTA critical on 26/11/2008, prior to an Earthquake M=4.2 on 29/11/2008, then continuing the analysis there is another critical point on 29/11/2008)



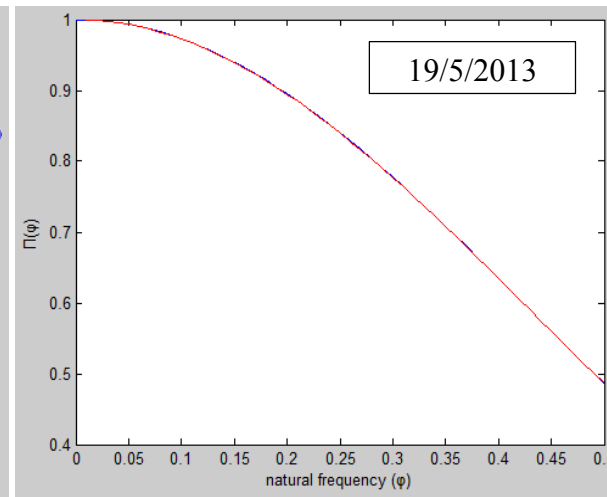
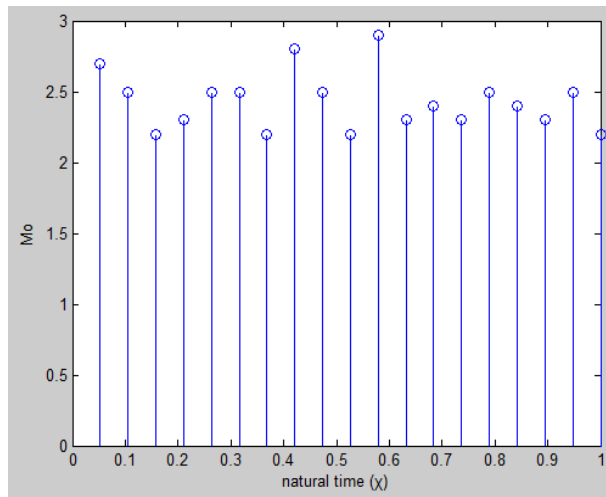
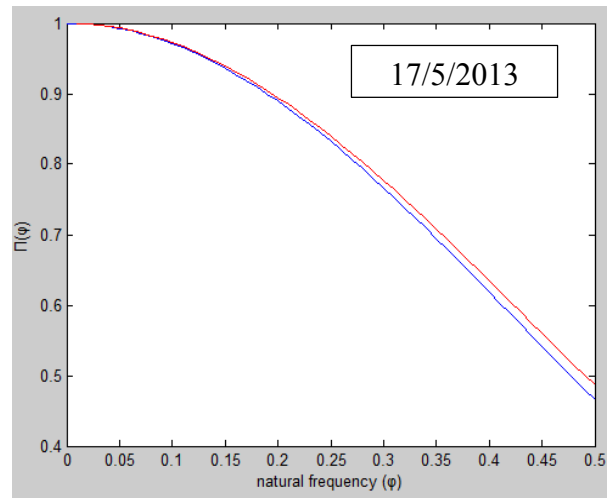
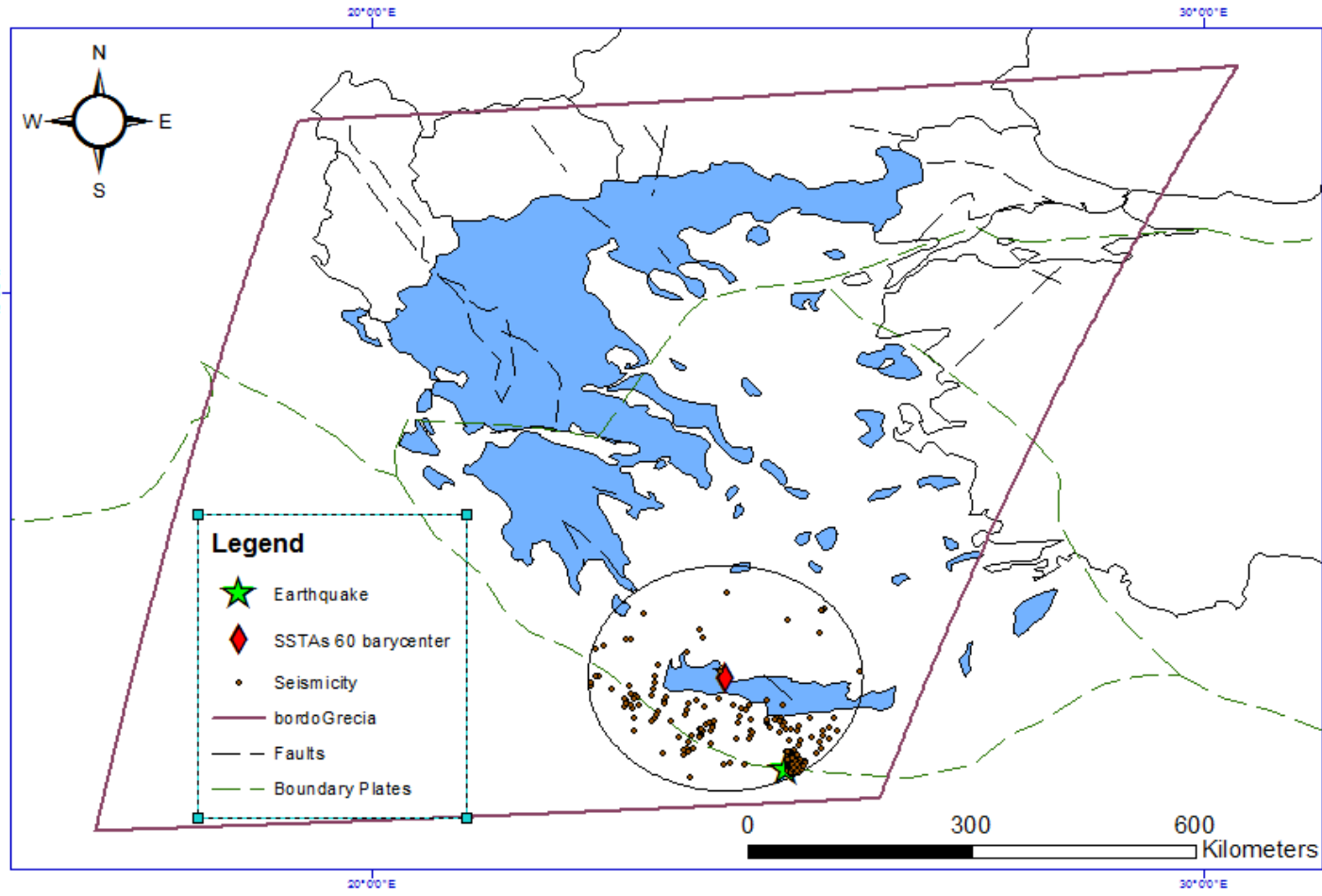
SSTAs 37 (Ionian-Peloponnese-Central) on 1,2,4,6,7,9/1/2010 Earthquake on 18/1/2010 M=5.2



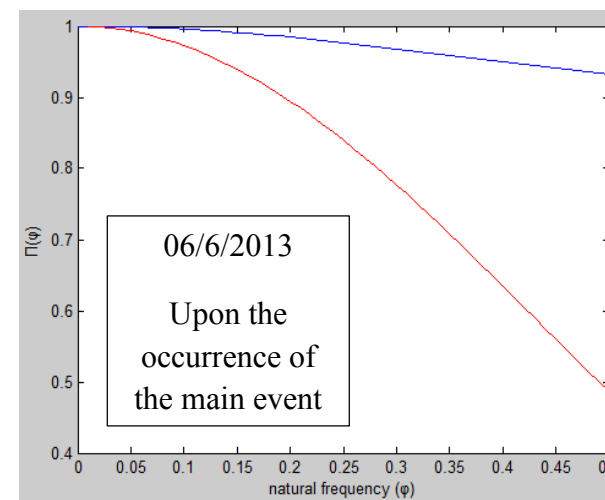
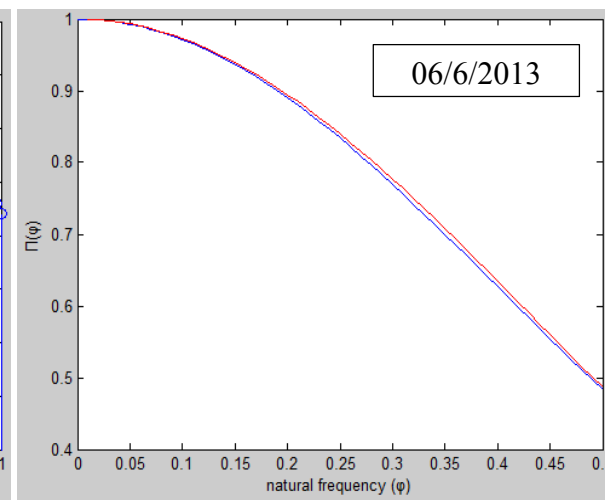
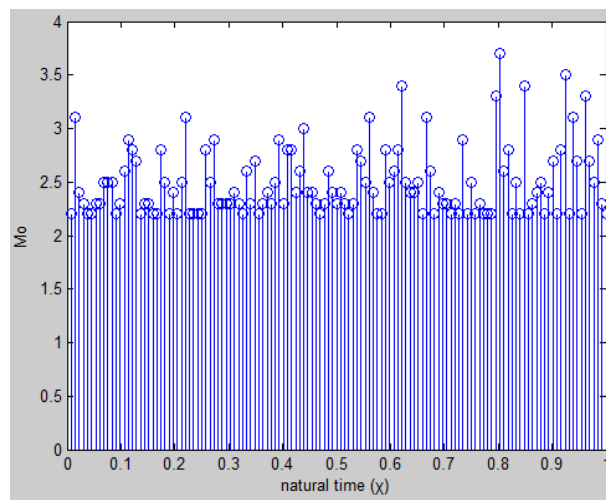
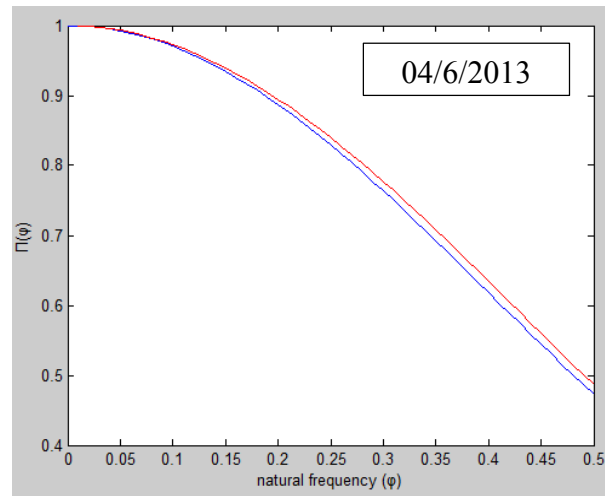
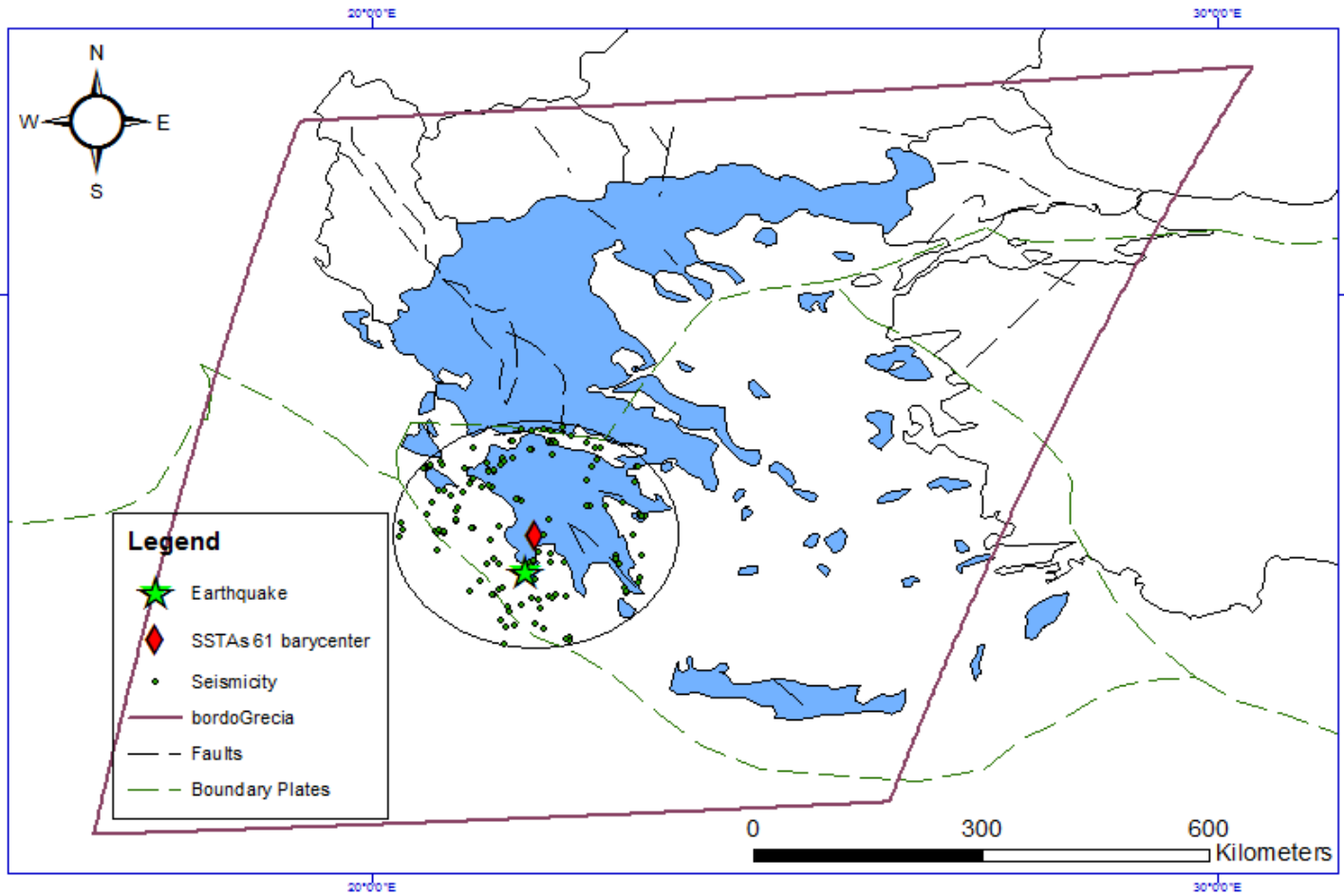
SSTAs 38 (Ionian-Peloponnese-Central) on 25-28/2 and 2,5/3/2010 Earthquake on 9/3/2010 M=5.1



SSTAs 60 (Crete-Mediterranean-Aegean) on 27-29/5/2013 Earthquake on 15/6/2013 M=5.8



SSTAs 61 (Ionian-Peloponnese-Central) on 27,29,30/5/2013 Earthquake on 6/6/2013 M=5.0



SSTAs 62 (Ionian-Peloponnese-Central) on 2,3/10/2013 Earthquake on 12/10/2013 M= 6.2

